Copyright Warning & Restrictions

The copyright law of the United States (Title 17, United States Code) governs the making of photocopies or other reproductions of copyrighted material.

Under certain conditions specified in the law, libraries and archives are authorized to furnish a photocopy or other reproduction. One of these specified conditions is that the photocopy or reproduction is not to be "used for any purpose other than private study, scholarship, or research." If a, user makes a request for, or later uses, a photocopy or reproduction for purposes in excess of "fair use" that user may be liable for copyright infringement,

This institution reserves the right to refuse to accept a copying order if, in its judgment, fulfillment of the order would involve violation of copyright law.

Please Note: The author retains the copyright while the New Jersey Institute of Technology reserves the right to distribute this thesis or dissertation

Printing note: If you do not wish to print this page, then select "Pages from: first page # to: last page #" on the print dialog screen

ABSTRACT

NON-DESTRUCTIVE EVALUATION OF AGGLOMERATED CORK PRODUCTS USING THZ SPECTROSCOPY AND IMAGING

by
Han Zhang

Terahertz spectroscopy from 0.15 to 0.3 THz is used to classify agglomerated cork products. Position dependent scattering of radiation allows one to image the internal structure of cork products. Previous studies have focused on natural (solid) cork stoppers. In this study, the feasibility of classifying agglomerated cork structures using THz imaging and spectroscopy is investigated. Both THz images and spectra are used to classify the agglomerated cork samples. Classification of the samples used three methods: visible examination of the THz images, statistical analysis of the pixel intensities, and a polynomial regression of the THz spectral data averaged over all pixels. Three types of agglomerated corks are studied: large cork granule, small cork granule, and twin-top technical corks. Classification based on both THz absorbance and time-delay enables the classification of the three cork types. Eventually, the measured THz properties and classifications will be correlated with the corks' measured oxygen transfer rate, which is an important performance criterion.

NON-DESTRUCTIVE EVALUATION OF AGGLOMERATEDCORK PRODUCTS USING THZ SPECTROSCOPY AND IMAGING

by
Han Zhang

A Thesis
Submitted to the Faculty of
New Jersey Institute of Technology
and Rutgers, The State University of New Jersey – Newark
in Partial Fulfillment of the Requirements for the Degree of
Master of Science in Applied Physics

Federated Department of Physics

January 2012

APPROVAL PAGE
NON-DESTRUCTIVE EVALUATION OF AGGLOMERATED-CORK PRODUCTS USING THZ SPECTROSCOPY AND IMAGING

Han Zhang

Dr. John F. Federici, Thesis Advisor Distinguished Professor of Physics, NJIT	date
Dr. Tao Zhou, Committee Member Associate Professor of Physics, NJIT	date
Dr. Robert B. Barat, Committee Member Professor of Chemical Engineering, NJIT	date
Dr. Caroline Brisson, Committee Member Assistant Professor of Engineering Physics, Ramapo College of New Jersey	date

BIOGRAPHICAL SKETCH

Author: Han Zhang

Degree: Master of Science

Date: January 2012

Undergraduate and Graduate Education:

- Master of Science in Applied Physics
  New Jersey Institute of Technology, Newark, NJ, 2012

- Bachelor of Science in Applied Physics
  South China University of Technology, Guangzhou, P. R. China, 2010

Major: Applied Physics

Acknowledgements

This thesis could not have been written without Dr. Federici who not only served as my advisor but also encouraged and challenged me throughout my graduation program. He provides me with unfailing support, encouragement and guidance at every step of my studies.

My heartfelt thank goes to the distinguished committee members Dr. Robert Barat, Dr. Tao Zhou and Dr. Caroline Brisson who reached out in every possible ways to support this endeavor of mine by providing critical comments and invaluable suggestions.

I also gratefully acknowledge Amorim & Irmaos, SA of Portugal for supplying the agglomerated cork samples for the THz studies presented in this thesis.

TABLE OF CONTENTS

LIST OF TABLES

LIST OF FIGURES

CHAPTER 1

INTRODUCTION

1.1 Background

Terahertz (THz) radiation refers to electromagnetic waves propagating at frequencies from 0.1 to 10 THz. It lies between microwave and optical frequencies in the electromagnetic spectrum as shown in Figure 1.1. It was not until recently that scientists began to widely use THz radiation since efficient and affordable THz sources and detectors have only been developed in the last ten years. In the past few years, THz technology has been applied in a range of fields like bio-medical imaging, quality assessment and material characterization, etc. [1-4] In the meantime, research on THz technologies has grown steadily. In the field of quality assessment, THz technology, taking advantage of its unique feature of non-destructive yet penetrating radiation, is very promising. One of the objectives for THz non-destructive testing is to investigate the interaction of THz beams with materials of interest and classify their response to THz radiation. The magnitude and phase of THz radiation which is transmitted through a material will depend not only on material's thickness and intrinsic absorption coefficient but also on the scattering of THz radiation by structural imperfections in the material. A second objective for non-destructive evaluation using THz technology is to correlate a material's THz properties – nominally corresponding to the measured phase and amplitude of the transmitted THz radiation - to some aspect of the material's or products' quality. If a link between the product's THz properties and its performance can be identified, then automatic product examination and classification could be realized. In this thesis, the focus

is on the interaction of THz radiation with agglomerated cork products and classification of the agglomerated cork products by their THz signatures.

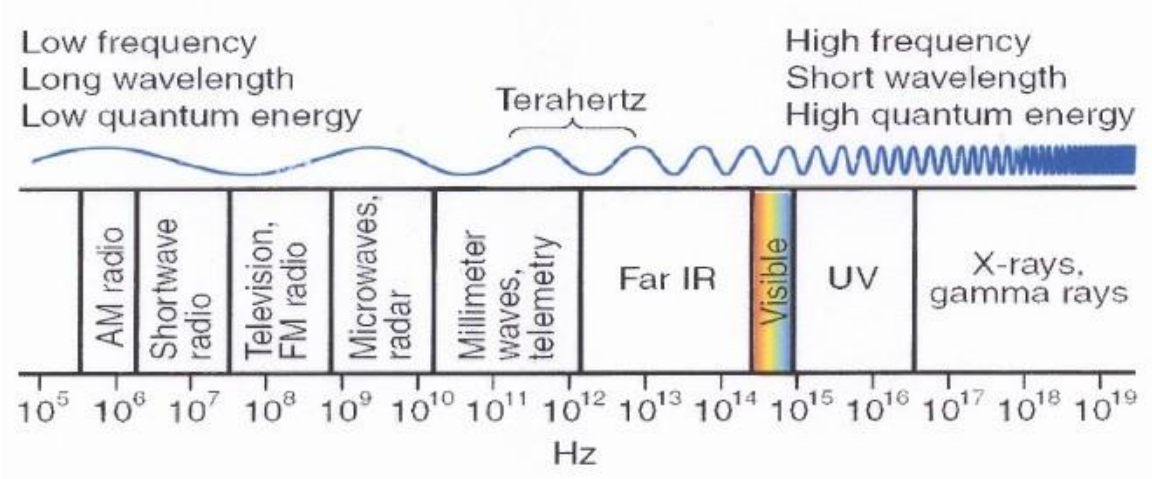

Figure 1.1 Electromagnetic spectrum and THz frequency range.[5]

There are various kinds of cork stoppers available.[6] But agglomerated cork stoppers which are formed out of natural cork are considered to be the most efficient and economic among all the kinds of cork stopper. [7] The agglomerated cork stoppers are formed from granulated cork which is derived from the natural cork. Agglomerated cork stoppers can be manufactured by individual molding or by extrusion. In both methods, approved food contact glues are used to bind the cork granules together. So called "technical cork stoppers" are comprised of agglomerated cork stoppers with natural cork disks being attached at both ends of the stopper. Both technical and agglomerated cork stoppers are classified as agglomerated cork stoppers. As enclosures for liquids, cork has the property of being impermeable to liquids and gases, as well as compressible. The quality of agglomerated cork stoppers is determined by the size of granular components, the quality of granulated cork, *etc*. Agglomerated cork stoppers of poor quality may affect the taste of wine. [8] Methods of non-destructive evaluation (NDE) of cork products

include visible inspection either by human experts or camera systems [6, 9], chemical analysis (including cork soaks) for the presence of trichloroanisole (TCA) [10-12], x-ray tomography [13], and THz imaging and spectroscopy [14, 15].

1.2 Objective

In this thesis, Terahertz (THz) imaging and spectroscopy is used as a NDE tool to characterize and classify agglomerated cork products. The potential of THz spectroscopy and imaging for NDE of natural cork enclosures [14, 15] is well stated. The large volume of gas (~80-95%) and relatively low humidity (~7%) enclosed by the cork cells enables the material to be compressible, yet exhibit fairly high THz transmission.

In this thesis, the interaction of THz radiation with agglomerated cork stoppers is detailed and the use of THz imaging and spectroscopy for NDE of cork quality is emphasized. Since the cork cells contain mostly gas, they are fairly transparent to THz radiation particularly in the low frequency THz range. Position dependent scattering of radiation allows one to image internal property of cork products. [14, 15] The sample preparation and experimental setup is detailed in Chapter 2. In Chapter 3, results, THz images, analysis and methods of classification are described. Conclusions and future outlook of this work are summarized in Chapter 4.

CHAPTER 2

Experimental Setup

2.1 Samples

Three types of agglomerated cork products, supplied by Amorium & Irmaos, SA, are tested. Each type includes 20 cork samples. The first cork products labeled as ‘A’ corks are made of large-sized cork granules. The second kind labeled as ‘N’ corks are made of small-sized cork granules. The third kind labeled as ‘TT’ corks are twin-top technical corks made of large-sized cork granules in the middle agglomerated section with two natural cork discs glued on both the top and bottom of the stopper. Samples of each kind are roughly 42, 43 and 44mm long with the same diameter of 23mm. For A and TT corks, Fabricol Ag202 L lote 111309 glue is used while for N corks, either Biocol BS30R or Flexpur 280A glue is used.

2.2 Devices

A T-Ray 2000 spectroscopy system (Picometrix, Inc.) is used in the transmission mode to measure the THz time-domain waveform. It consists of a diode-pumped solid state laser emitting <80 fs at 800 nm, a grating dispersion compensator (GDC) to compensate for pulse broadening in the fiber-optic cables, a T-Ray control Unit which controls the delay stages, and a THz transmitter and receiver. The schematic of the system is shown in Figure 2.1. A pair of silicon lenses (3 inch focal length) focuses the THz radiation to a spot at which the sample is placed. The imaging system consists of a computer controlled vertical translation stage (1 μm resolution) and a computer controlled rotation stage (0.001 º resolution). Samples are placed on a hollow plastic mount with a pipe connecting to a small

vacuum pump. When suction is drawn by the pump, the sample is firmly held to the plastic mount. The plastic mount is fixed on the computer controlled rotation stage. The schematic of the setup is shown in Figure 2.2. The THz beam is aligned so that it always passes through the diameter of the cork stopper as the sample is scanned. The THz images are acquired by recording the THz transmitted pulse through the sample for each rotation angle and vertical height position.

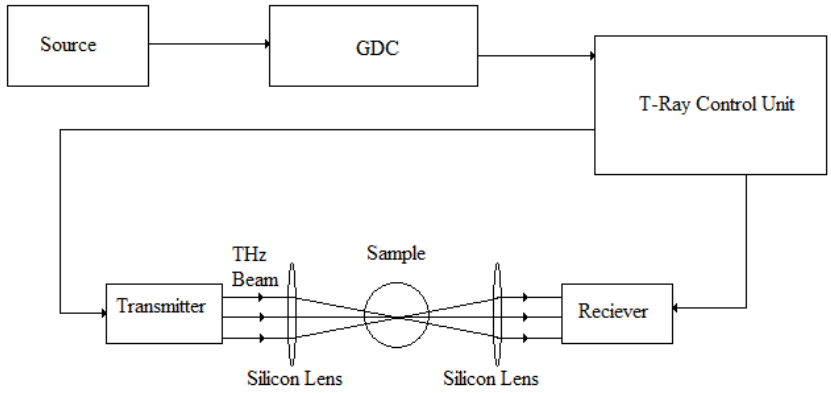

Figure 2.1 The T-Ray 2000 System.

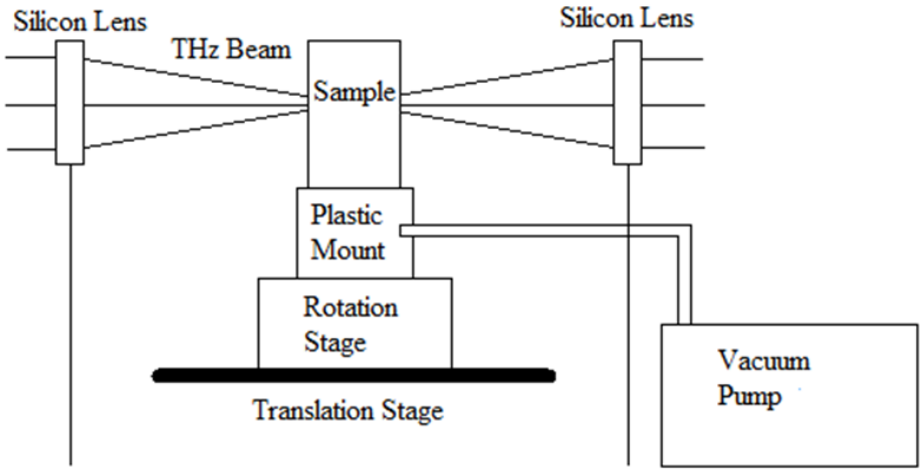

Figure 2.2 Illustration of sample mounting to rotation stage. The sample is moved vertically to scan the THz beam through different vertical heights of the cork. The rotation stage moves in 2 degree increments from 0 to 180 degrees of rotation. The step size of the vertical scan is 0.5mm.

2.3 Sample Data

Typical THz time domain waveforms are shown in Figure 2.3. The reference waveform is acquired with the cork removed. As shown in Figure 2.3, there is a time shift in the arrival of the peak of the pulse through the cork relative to the reference waveform. The time shift is indicative of the cork's real index of refraction. The reduced amplitude of the THz waveform relative to the reference waveform is indicative of absorption or scattering of the THz waveform by the cork.

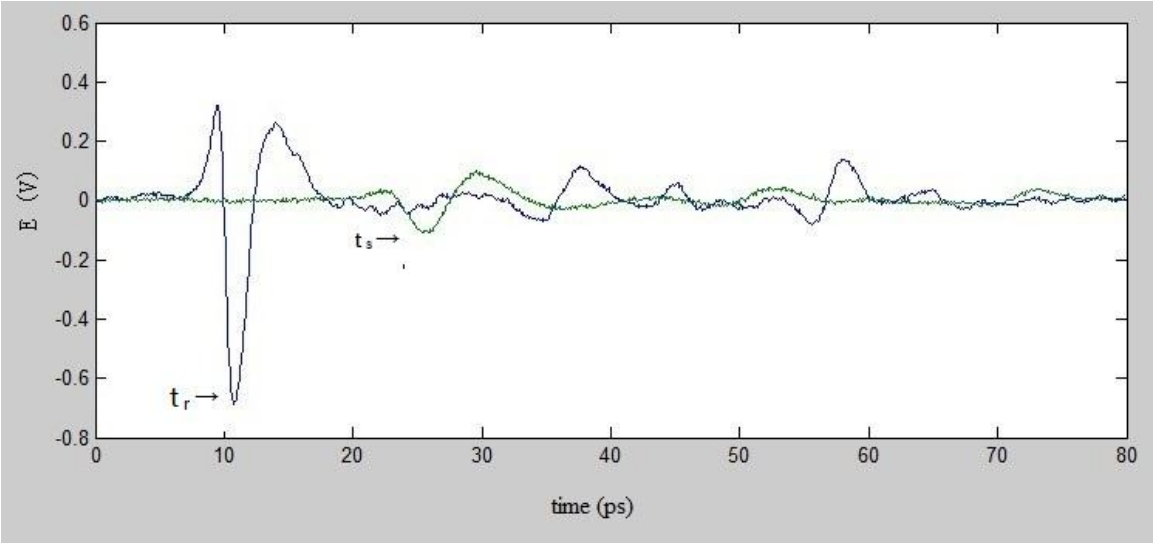

Figure 2.3 Measured THz time-domain waveform (green) through an agglomerated cork product sample. The reference waveform (black) is taken with the sample removed. The arrows in the figure indicated the location of the minimum peak values for both the reference and sample waveforms.

Spectral information of both the phase and amplitude is acquired through a Fourier transform of the time-domain data. The corresponding amplitude as a function of frequency can be calculated by Fourier transforming the time-domain data as shown in Figure 2.4. In examining the magnitude of the THz electric field as a function of frequency (Figure 2.4), it is clear from the reference data that the THz amplitude approaches the noise

limit of the THz system at approximately 1.5THz. After passing through the cork sample, data beyond ~0.3THz is in the noise for this particular sample location. Typically the lower limit for the THz system is ~0.1THz.

THz images are formed by measuring the full time-domain waveform within an 80 ps time window. The sample is aligned such that the THz beam always propagates through the diameter of the cork. The sample is mechanically scanned vertically (along the axial direction of the cylindrical cork) by a linear translation stage. Different angles of the sample are measured as the rotation stage rotates step by step. The image is acquired one pixel at a time. The vertical step size is 500 μm while the angular step size is 2 º.

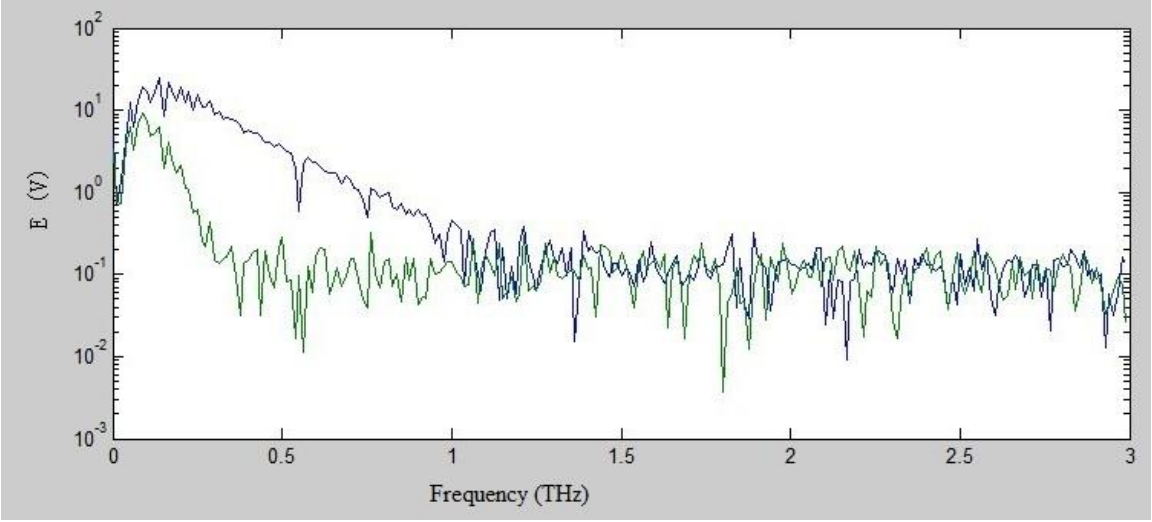

Figure 2.4 Corresponding amplitude as a function of frequency after Fourier transforming the time-domain data. Sharp structures near 0.57, 0.7, and 1.1THz in the reference waveform are artifacts of absorption by water vapor in the atmosphere.

CHAPTER 3

RESULTS AND DISCUSSION

3.1 Analyzing Method

There are various methods for analyzing the THz waveforms and generating a THz image. For example, one can measure the total transmitted THz power, the transmitted power within a given frequency interval, *etc*. In this thesis, frequency dependent optical constants and the time-delay of the THz pulse through the cork are investigated. At each pixel in the THz image, the THz phase and amplitude is normalized to the phase and amplitude of the reference waveform. Figure 3.1 shows the corresponding absorbance

$$A(v) = -ln\big(T(v)\big) = -ln(\frac{|E_s(v)|}{|E_r(v)|}) \tag{3.1}$$

for each pixel, where $T(v)$ is the frequency dependent transmission referenced to a THz spectra with the sample removed. $|E_s(v)|$ and $|E_r(v)|$ are the frequency dependent magnitudes of the THz electric fields for sample and reference, respectively. Figure 3.1 also shows that for this particular pixel, the preferred frequency range is between 0.1 to 0.3THz. Outside of this range noise dominates the signal.

The time delay of the time-domain THz waveform can be calculated by

$$t_d = t_s - t_r \tag{3.2}$$

where t_s and t_r are the times of the minimum pulse value for the sample and reference, respectively. This is a rather easy and efficient way to generate the THz image while the disadvantage is a loss of spectral information.

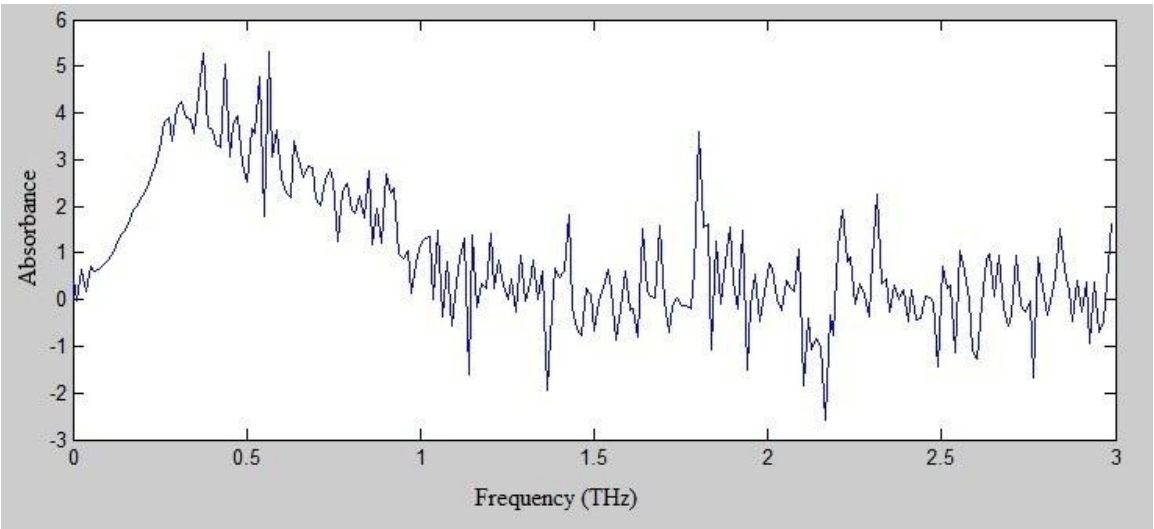

Figure 3.1 Frequency dependent absorbance for the time-domain waveform of Figure 2.3

3.2 Visible and THz Images

Some visible and typical THz images of cork samples are shown in Figure 3.2 – 3.4. The THz images are formed by calculating the average absorbance in different frequency intervals or by calculating the time delay. The THz beam always goes through the center (diameter) of the sample as it rotates such that the horizontal direction of the THz image corresponds to the rotation angle while the vertical direction corresponds to the axial height in the cylindrical cork. The samples are initially oriented so that the label on the sample is facing towards the incident THz beam. The sample rotates 180 ºcounter-clockwise so that when the rotation ends, the mark on the sample is facing away from the incident THz beam.

THz images can also be generated based on the time delay in the arrival of the THz pulse. From the time delay of ~15ps from Figure 2.3 through a 23mm cork, it can be estimate that a typical index of refraction should be approximately 1.18. The time-delay THz images show the presence of similar structures as the THz amplitude images.

However, when using the time delay image data for statistical analysis, one must consider some experimental limitations in determining the time delay. Since the arrival time is determined by the optical path length, a slight variation of the cork sample position would affect the data. Each cork is manually centered on the THz beam. It is possible that each sample may not be exactly placed such it is centered on the THz beam. If the cork were placed 1mm off-center, then the geometric length through the sample would decrease by 0.08 mm. For a real refractive index of the cork of ~1.18, the corresponding the time delay would decrease by ~0.03 ps. Since a typical time-delay is ~15ps, the error in the time-delay due to slight misalignments of the cork is negligible.

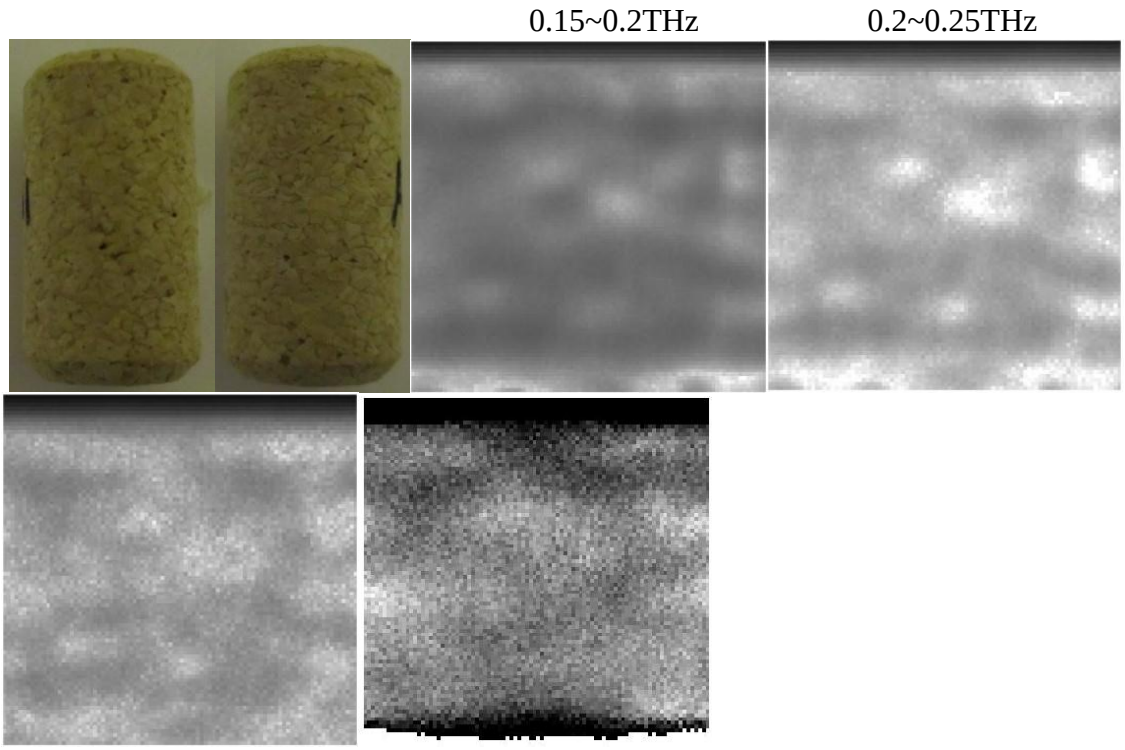

Figure 3.2 Visible image of A1 cork sample (top left). 0.15-0.2 THz image of A1 cork sample as black stands for absorbance of 0 and white stands for absorbance 4 and higher (top middle). 0.2-0.25 THz image of A1 cork sample as black stands for absorbance of 0 and white stands for absorbance and 4 and higher (top right). 0.25-0.3 THz image of A1 cork sample as black stands for absorbance of 0 and white stands for absorbance of 6 or higher (bottom left). Time delay THz image of A1 cork sample (bottom middle).

For the THz time-delay images, the maximum time delay was set as white and minimum time delay as black to show the maximum contrast. Comparing the visible and THz images, it can be shown that all three types of agglomerated cork samples do not appear uniform in the THz images. Internal structures could be caused by variations in the structure within an individual cork granule, or variations in the collection of granules, or hole/ voids between the granules. Variations in the measured absorbance in a set frequency interval are clearly observable in the THz images.

Figure 3.2 is for the A1 cork sample. Excluding the top and bottom of the THz image which correspond to the edges of the sample, there are some white regions in the middle in all of the THz images for both amplitude and phase. This implies that for those locations the absorbance is higher. For these same locations, it takes more the time for the THz beam to travel through these regions. Such regions may indicate variations in the cork granule qualities, size, or other properties.

Figure 3.3 is for the N1 cork sample. The THz images are much more uniform in brightness than those of the A1 cork sample because the cork granules of N samples are much smaller in size. Also from the 0.2-025 and 0.25-0.3 THz image vertical lines can be noticed which appear in the images. These lines are an artifact resulting from a limited signal-to–noise ratio at these frequencies. Therefore, when the THz images are analyzed numerically, the frequency range between 0.15-0.2 THz will be focused to eliminate the experiment artifact.

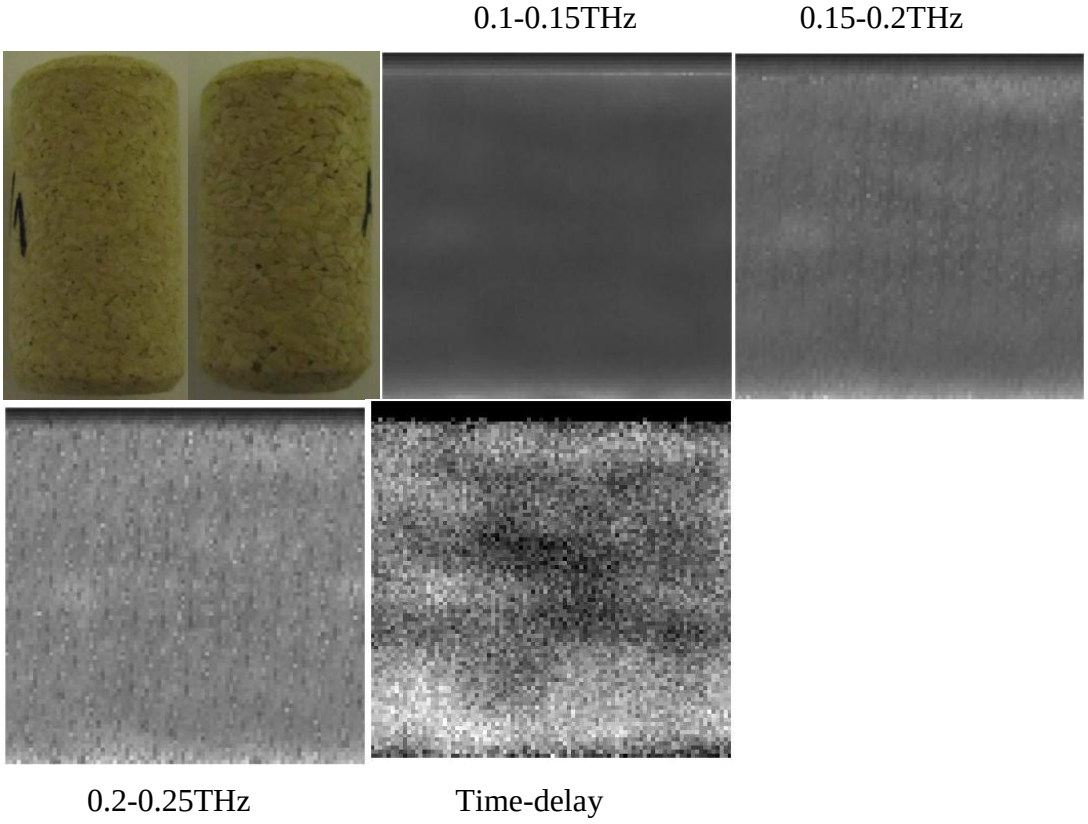

Figure 3.3 Visible image of N1 cork sample (top left). The next three images corresponds to a 0.15-0.2 THz, 0.2-0.25 THz, and 0.25-0.3 THz image of N1 cork sample where black stands for absorbance of 0 and white stands for absorbance of 6 and higher. The time delay THz image of N1 cork sample is shown in the bottom middle. Vertical lines in the images are experimental artifacts. Analysis will be restricted to the 0.15-0.2 THz range so that the artifact is not present in any of the data.

Figure 3.4 is for the TT1 cork sample. The THz images clearly show the top and bottom cork discs. The visible holes in the cork structure (marked in the top middle images) when viewed from the bottom have regions of correspondingly THz high absorbance. Both the top and bottom cork discs' absorbance are less than the middle part which indicates that the homogeneity of the cork disks is generally better than the agglomerated section of the cork which is comprised of not only the cork granules, but also

the presence of glue, or the boundaries of the granules. As with the A1 sample, the TT1 sample's middle part does not produce an image of uniform intensity.

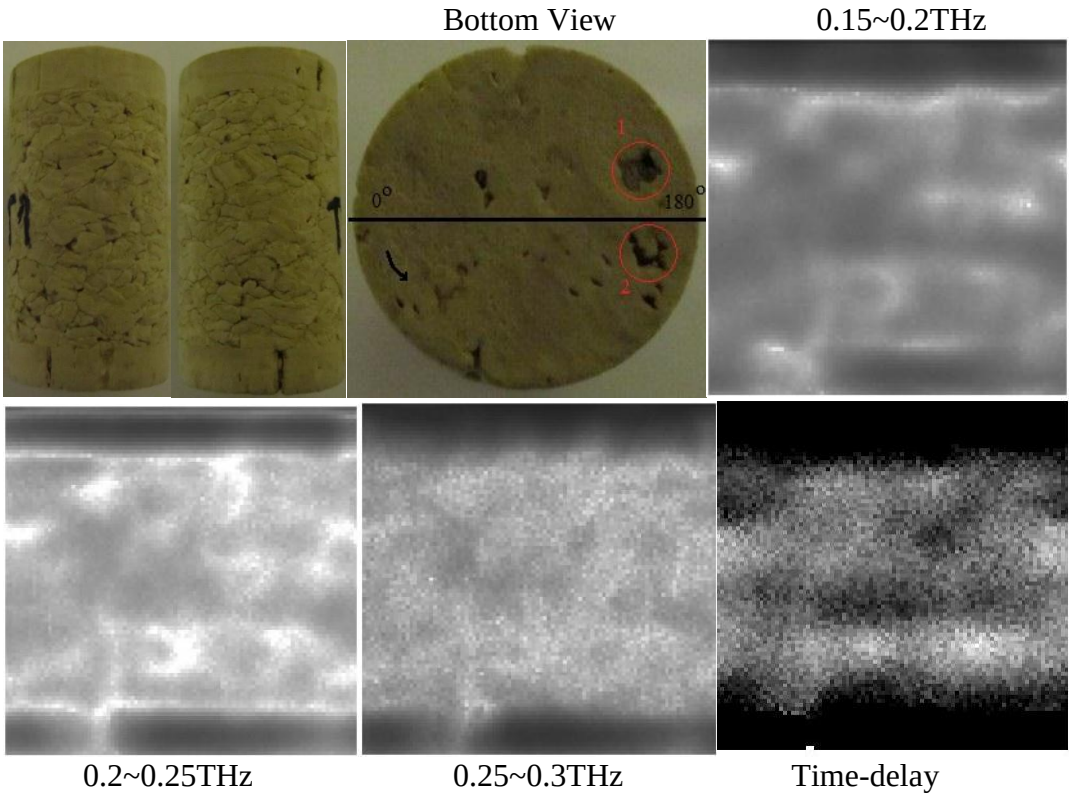

Figure 3.4 Visible image of TT1 cork sample (top left). Visible image of the bottom disc of TT1 cork sample (top middle). Following two absorbance images correspond to 0.15-0.2 THz , and 0.2-0.25 THz in which black stands for absorbance of 0 and white stands for absorbance of 4 and higher, Bottom middle is a 0.25-0.3 THz image of TT1 cork sample in which black stands for absorbance of 0 and white stands for absorbance of 6 and higher. The time delay THz image of N1 cork sample is at the bottom right.

The first and simplest method which was used to classify the THz images was to visually inspect the THz images for a given class of corks (eg. A, N or TT as a group) and observe any large variations in the recorded THz images. This method was applied for all the 60 agglomerated cork samples. Generally, the THz images generated from samples of the same class shared similar features, with only one exception: cork N14.

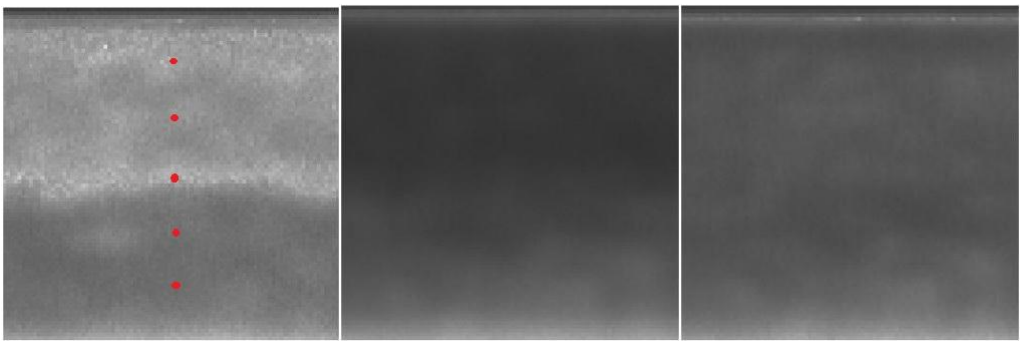

Figure3.5 N14 cork sample absorbance image in the 0.25-0.3 THz range White corresponds to absorbance of 6 and higher (left). 0.2-0.25 THz image for which white stands for absorbance of 4 and higher (middle). 0.15-0.2 THz image for which white stands for absorbance of 4 and higher (right). Red points on the left figure indicate the pixel investigated as discussed in the text.

Absorbance images of cork N14 are shown in Figure 3.5. In examining the 0.25-0.3THz absorbance image, there appears to be a high absorbance region in the top half and a low absorbance region in the bottom half of the cork. Some particular pixels of the N14 sample are picked as indicated in Figure 3.5 to analyze its absorbance as shown in Figure 3.6. The absorbance increases slowly between 0.1 and 0.2 THz. Then absorbance varies for different pixels when the frequency is above 0.2 THz. At this point, it is difficult to assign with certainty the origin of the spectral anomalies in Cork N14. One possibility is that the features may result from enhanced scattering of the THz radiation by the cork granules and glue due to pockets of air which are trapped in the cork.

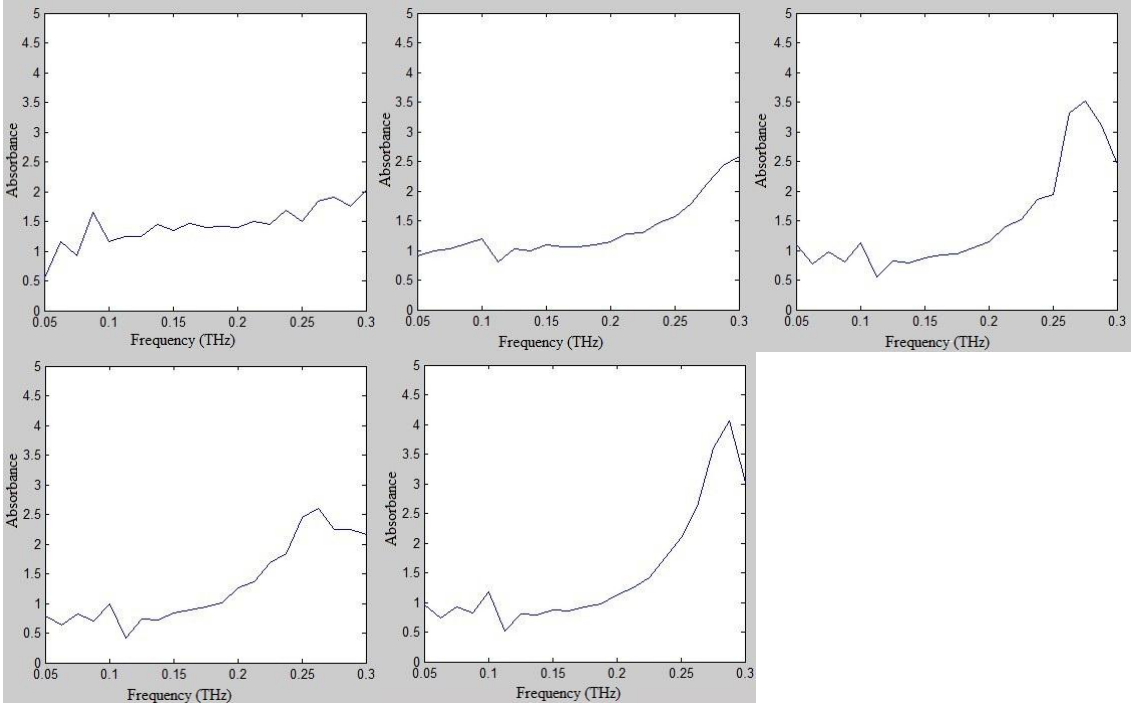

Figure 3.6 Absorption spectra from selected heights (y pixel =15,30,45,60,75) of cork N14 at a fixed rotation angle of 90 º, (left to right, top to bottom progression). Pixels of y15, 30 are in the darker region in the first image of Figure 3.5. Pixel of y45 is roughly in the middle of the cork on near the edge of the high absorbance region on the white stripe. Pixel of y60, 75 are in the brighter region.

Aside from the N14 spectral anomalies of Figure 3.6, analysis of the absorbance for all the other samples yields similar features to that shown in Figure 3.1. The absorbance between 0.05 and 0.3 THz increases with frequency which may be fit to a second order polynomial,

$$A(v) = Bv^2 + Cv + D \qquad (3.3)$$

where $A(v)$ is the frequency dependent absorbance, v is the THz frequency, and B, C and D are fit parameters. Data above 0.3 THz is dominated by noise and is excluded from the analysis. A best fit to the experimental data in Figure 3.1 is shown in Figure 3.7.

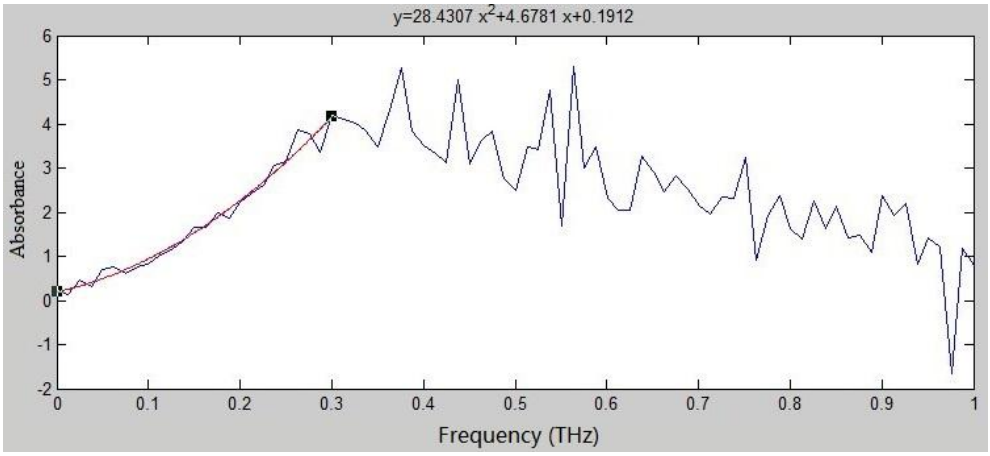

Figure 3.7 Fit polynomial for absorbance in figure 3.1. The absorbance is measured from A1 cork sample at pixel (angle20 º, y20). Extracted parameters: B = 28.4307, C = 4.6781, D= 0.1912

Glue used in the agglomerated cork samples is measured for its absorbance. Glue samples are prepared by curing samples roughly 1 cm thick. The measured absorbance results are shown in Figure 3.8. The absorption coefficients are about 1, 1.5 and 1.5 cm^{-1} at the frequency 0.15 THz for the glue sample Ag202 L lote 111309, Flexpur 280A and Biocol BS30R. For A and TT corks, the average absorption coefficient through the diameter of the cork sample is about 0.7 cm^{-1} (absorbance measured divided by the diameter of the sample) at the frequency 0.15 THz. For one granule, the thickness is about 2 mm and the granule is surrounded by glue with thickness of 200 μm. The overall attenuation for each cork should then be approximated by

$$A_{overall} = N(\alpha_{cork} * L_{cork} + \alpha_{glue} * L_{glue}) \qquad (3.4)$$

where N is the number of the granules through one diameter. Assuming N equals 11, the contribution of the glue to the absorbance is $\sim 11 \cdot 1.5 \cdot 200 \times 10^{-4} = 0.33$. The overall measured attenuation $A_{overall}$ for the cork sample is approximately 1.7, so that the contribution of the glue is about 20% of the total absorbance. This may indicate why the absorbance of the agglomerated cork is higher than that of the natural cork.

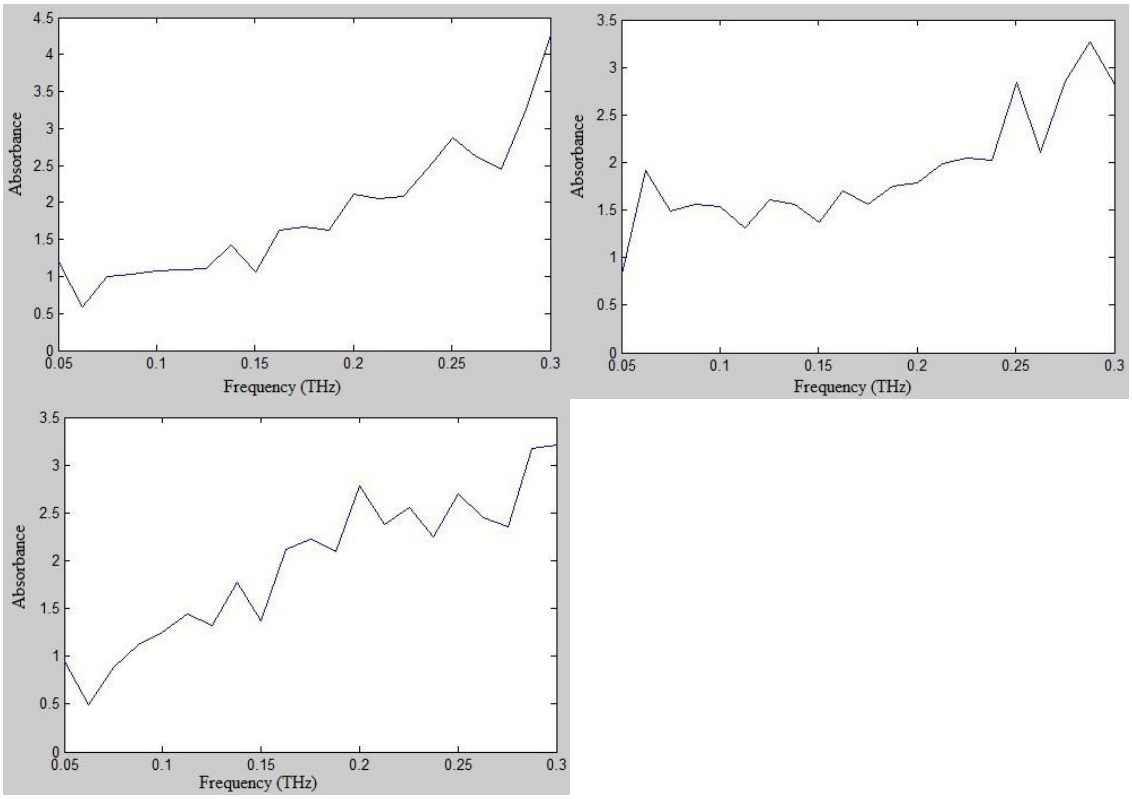

Figure 3.8 Measured frequency dependent absorbance of glue sample Fabricol Ag202 L lote 111309 (top left), Flexpur 280A(top right) and Biocol BS30R (bottom left)

3.3 Classification

Cork samples were classified in three ways. The first method was to classify the samples by a visual comparison of their THz images. It's direct and simple, while general structures can be identified. However, it is not very quantitative. The second method is to calculate the absorbance for all the pixels on the cork sample, analyze the statistical variation in the pixel values, and plot the histogram distribution. The third method is to calculate the average absorbance of all valid pixels for each sample as a function of THz frequency, fit

the spectral variation to a second order polynomial, and extract the coefficients to be classified.

3.3.1 Preliminary Classification of THz Images

THz images for A cork samples are shown in Figure 3.8. THz images for N cork samples are shown in Figure 3.9. THz images for TT cork samples are shown in Figure 3.10. All the images are generated in bandwidths from 0.15-0.2 THz. These images are on the same contrast scale such that black stands for absorbance of 0 and white stands for absorbance and 4 or higher. Time delay THz images for A, N, and TT cork samples are shown in Figure 3.11, Figure 3.12, and Figure 3.13. For these time-domain images, the contrast for each image is optimized to visualize the structure for each image. Because of the difference in data range between twin top discs and the agglomerated portion for time delay value, it's impossible to achieve good contrast for both parts in the time-delay images.

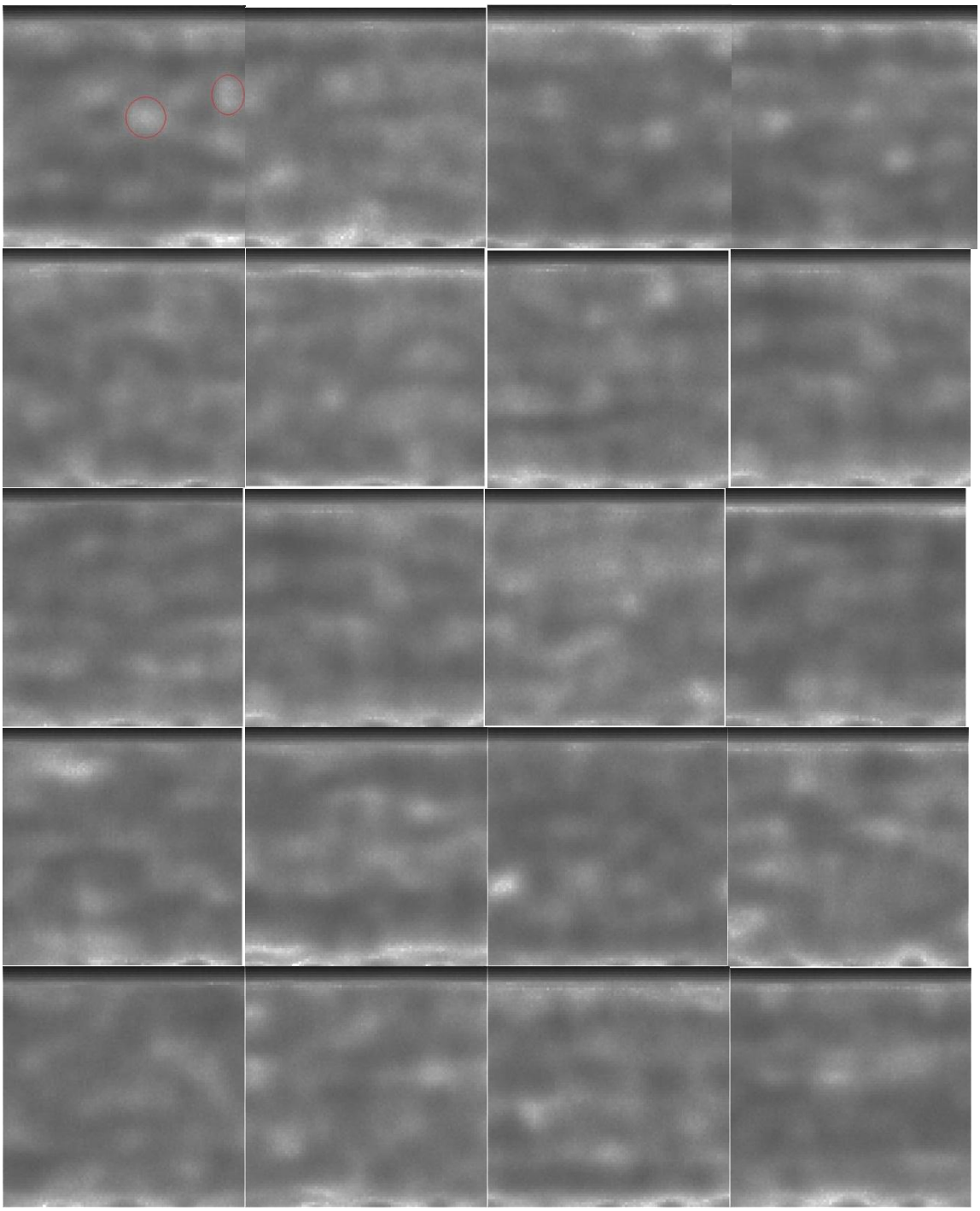

Figure 3.9 0.15-0.2 THz images of A cork sample (left to right, top to bottom progression) Typical bright spots on top left sample are circled in red.

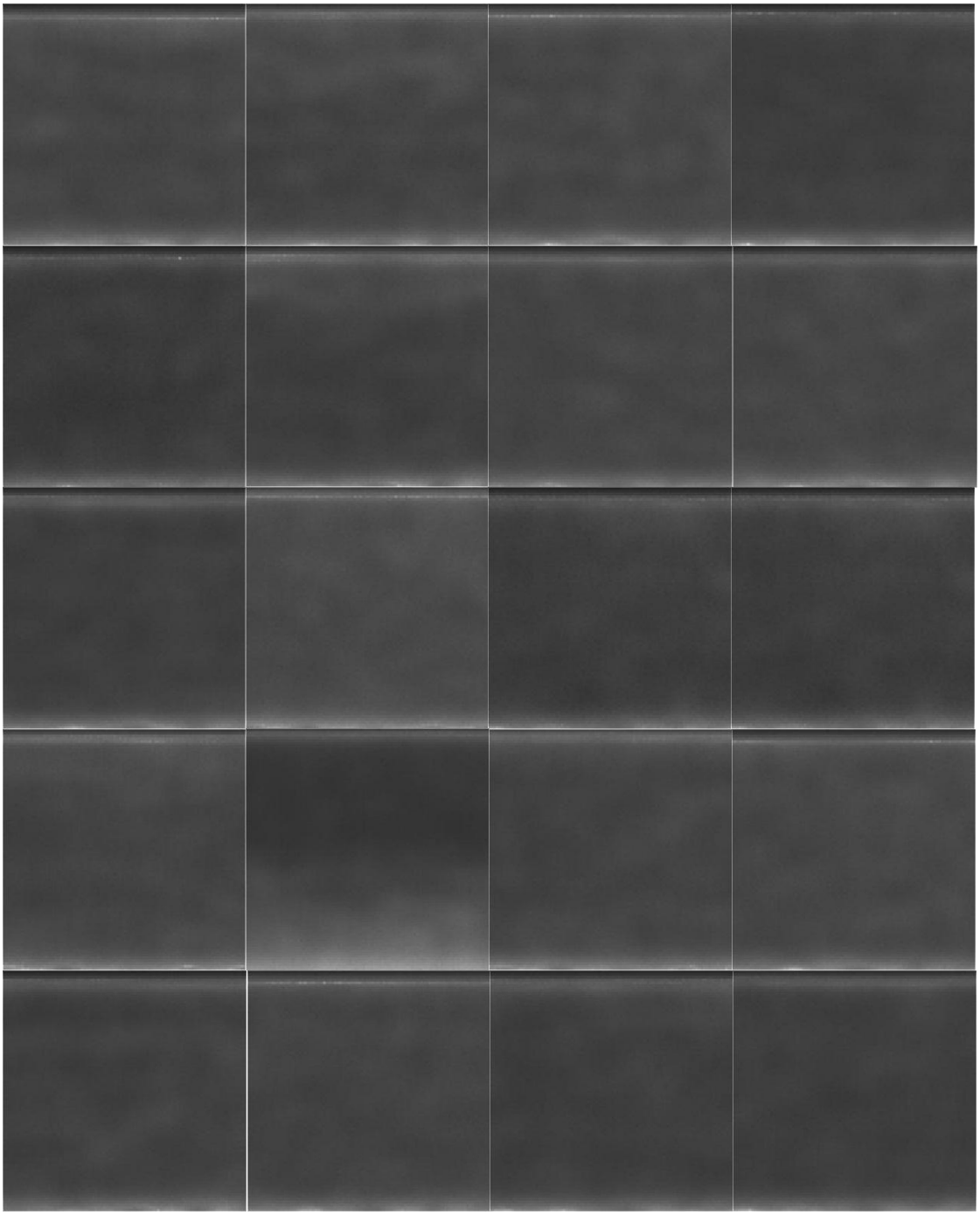

Figure 3.10 0.15-0.2 THz images of N cork sample (left to right, top to bottom progression)

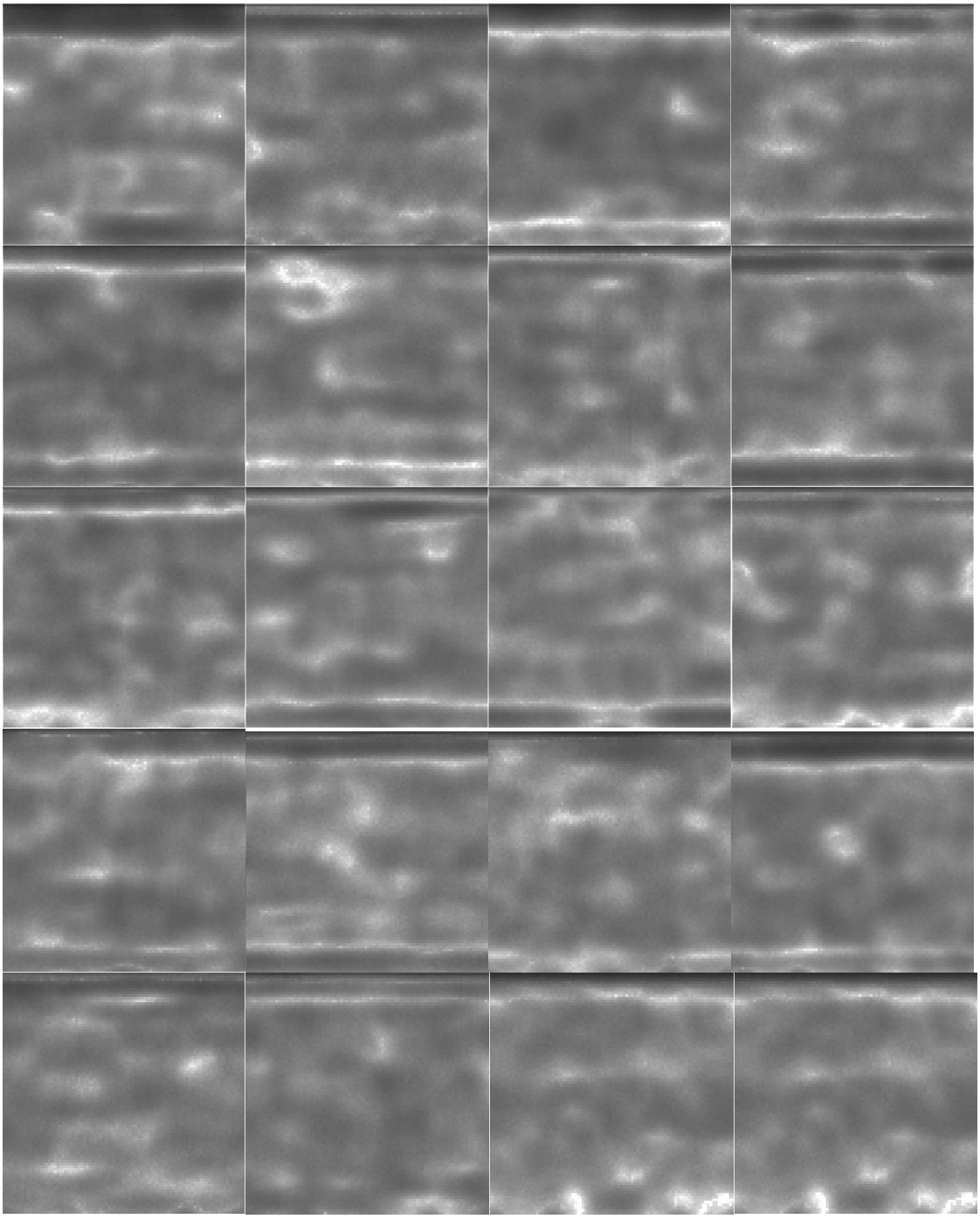

Figure 3.11 0.15-0.2 THz images of TT cork sample (left to right, top to bottom progression)

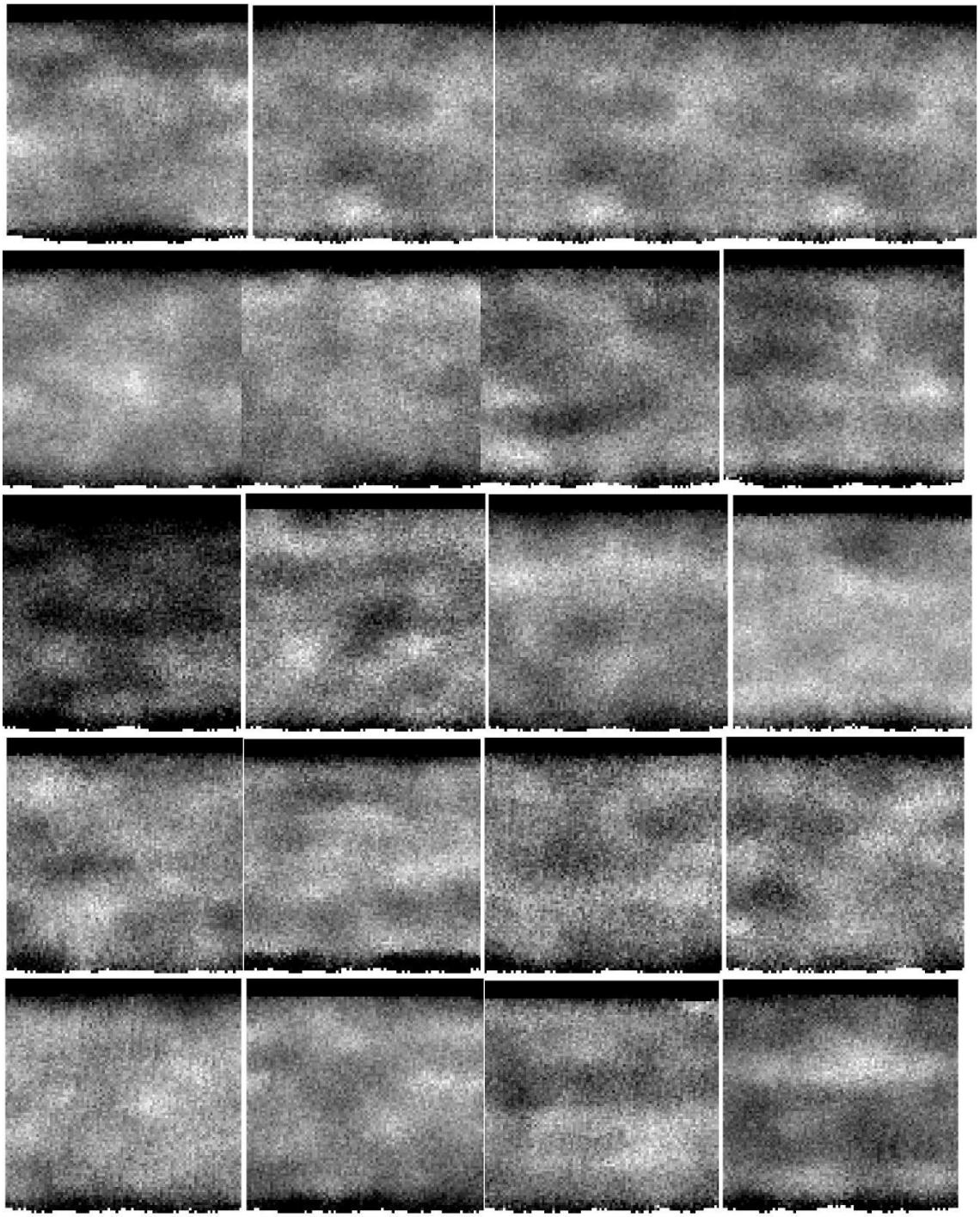

Figure 3.12 Time delay THz images of A cork sample (left to right, top to bottom progression)

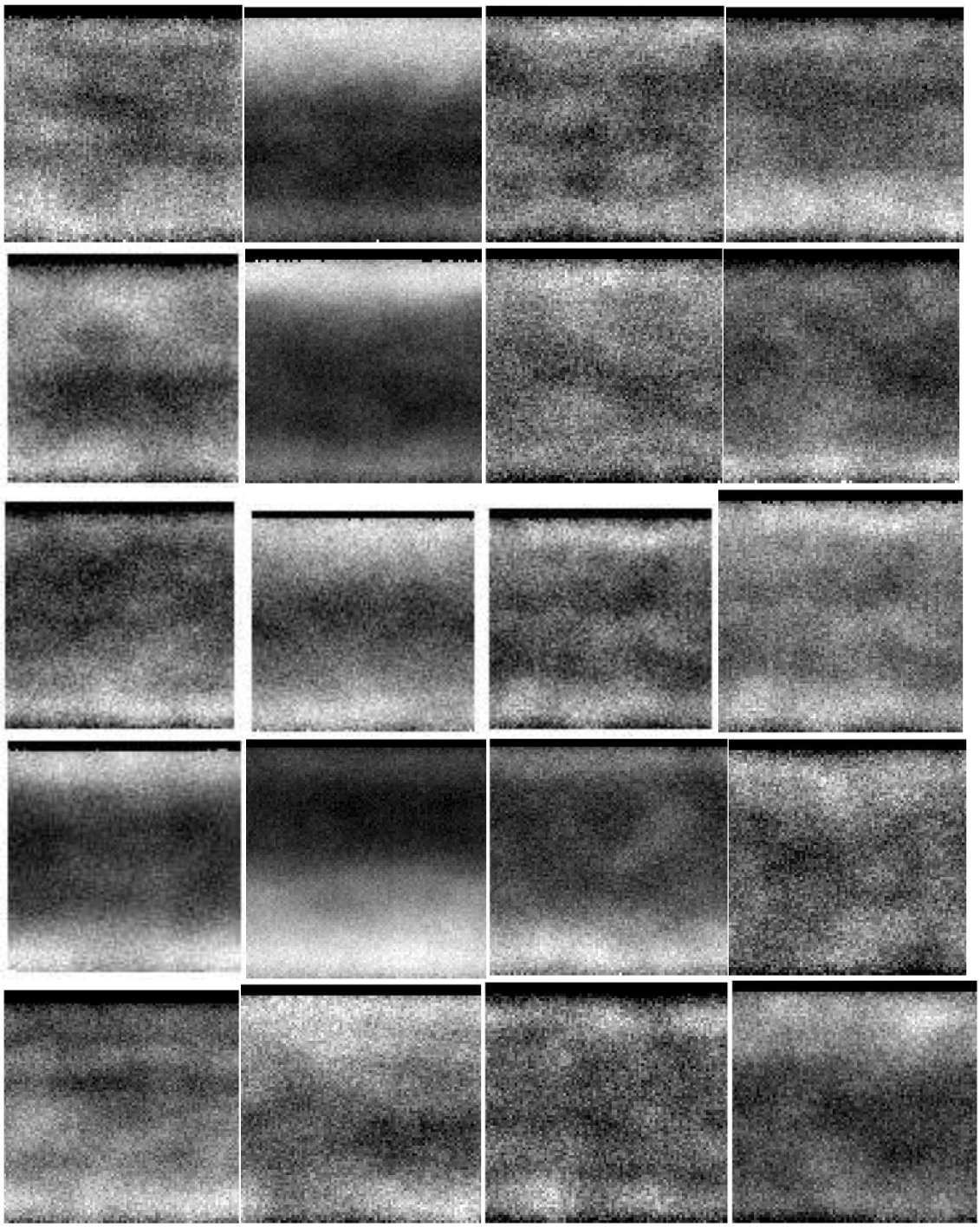

Figure 3.13 Time delay THz images of N cork sample (left to right, top to bottom progression).

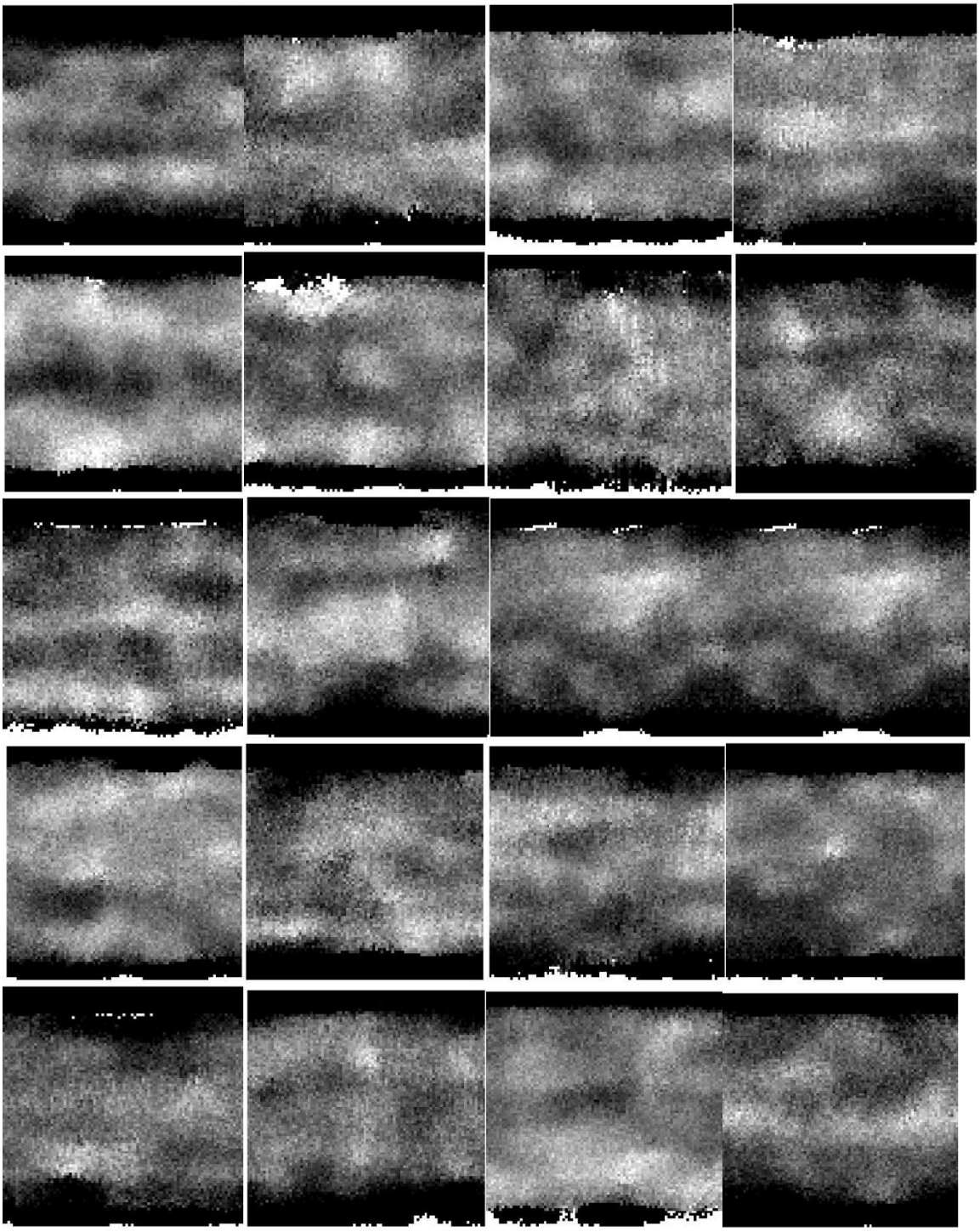

Figure 3.14 Time delay THz images of TT cork sample (left to right, top to bottom progression)

When examining the images, roughly 2mm from the top and bottom of the corks is excluded since the edges scatter the THz beam. For the A and the N corks, the bevel shape on the top and bottom of the cork samples are excluded from the analysis. For the TT corks, the granules in the middle portion of the cork are analyzed as well as the top and bottom cork disks. One can see that there is small contrast in the N cork absorbance images, all of which look generally uniform except for the N14 image which shows a different gray value between upper and lower part of the sample. For the same cork, regions of high absorbance also correspond to regions of large time delay.

As for the A corks, certain general structures can be discovered through these images. They can be divided into two categories: those have bright spots (circled in red on A1 image) including A1, A2, A3, A4, A7 A13, A15, A16, A18, A19, A20, and the rest which do not exhibit a bright spot. Such spots corresponding to high absorbance may be caused by higher mass density cork granules.

Similarly, TT corks can be divided in the same way with only TT5, TT7 and TT8 cork samples not exhibiting a bright spot. Samples with more than one spot are listed as follow: TT1, TT10, TT11, TT14 and TT15. TT cork samples also can be classified by its twin top natural cork discs. THz images of TT1, TT3, TT4, TT5, TT8, TT9 TT13, TT14 and TT16 samples show clear boundaries for both top and bottom discs while images of TT2, TT6, TT10, TT11, TT15, TT18, TT19 and TT20 samples only show a boundary for either the top or bottom discs. The rest of the images show no sharp boundary. Also, structure in the cork discs can be revealed through the THz image. Large holes in the cork disk (See Figure 3.4) are evidenced by regions of high THz absorbance. The results of the preliminary classification are listed in table 3.1.

Table 3.1 Results of Preliminary Classification

Samples	With bright spots	Without bright spot
A corks	A1, A2, A3, A4, A7 A13, A15, A16, A18, A19, A20	A5, A6, A8, A9, A10, A11, A12, A14, A17

Samples	With more than one bright spots	With one bright spot	Without bright spot
TT corks	TT1, TT10, TT11, TT14, TT15	TT2, TT3, TT4, TT6, TT7, TT9, TT12, TT13, TT16, TT17, TT18, TT19, TT20	TT5, TT7, TT8

Samples	With boundaries for both top and bottom discs	With boundary for either top or bottom discs	Without boundary
TT corks	TT1, TT3, TT4, TT5, TT8, TT9, TT13, TT14, TT16	TT2, TT6, TT10, TT11, TT15, TT18, TT19, TT20	TT7, TT10, TT11, TT12, TT17

3.3.2 Statistical Classification

The absorbance for each pixel in the image is calculated. Then, the mean absorbance, standard deviation, skewness and kurtosis for the set of pixels are calculated. The absorbance pixel data are taken from 0.15-0.2 THz transmission images. Results are listed in Table 3.2.

Table 3.2 Summary Statistics for Absorbance (0.15-0.2 THz Transmission) of Each Pixel for the Middle Part of A, N and TT corks

Sample	Mean	Standard Deviation	Skewness	Kurtosis
A1	1.818916	0.20173	0.881305	0.745003
A2	1.934963	0.1769	0.906024	1.989255
A3	1.780826	0.185834	1.420539	3.026338
A4	1.803555	0.173843	0.838523	1.593244
A5	1.850324	0.145714	0.573151	-0.00757
A6	1.915053	0.148467	0.594983	0.190384
A7	1.867273	0.162008	1.122566	2.497424
A8	1.822539	0.180698	0.758541	0.992095
A9	1.799689	0.14824	0.79141	0.434893
A10	1.822539	0.180698	0.758541	0.992095
A11	1.996044	0.174584	0.685338	1.10564
A12	1.732077	0.163483	0.845064	0.531531
A13	1.824903	0.218034	1.917616	4.951096
A14	1.858827	0.231687	1.294315	3.518296
A15	1.748332	0.177454	3.416418	18.81671
A16	1.906317	0.19034	1.1339	2.494092
A17	1.766043	0.1392	0.472174	0.123347
A18	1.875126	0.173925	1.238939	1.811021
A19	1.859019	0.180242	1.015937	1.361639
A20	1.782322	0.185617	0.847941	0.398158
N1	1.125899	0.081643	1.895847	4.042423
N2	1.117052	0.080615	0.61907	-0.30916
N3	1.141858	0.062717	1.438444	3.030025
N4	1.009137	0.058481	1.828904	4.60366
N5	0.951876	0.068866	1.473433	3.273326
N6	1.049059	0.101057	1.19011	0.817732
N7	1.10044	0.057658	1.839195	4.294356
N8	1.127241	0.065466	2.120543	5.664322
N9	1.005318	0.0658	2.219725	5.903212
N10	1.183925	0.065513	1.35257	2.568783

Table 3.2 Summary Statistics for Absorbance (0.15-0.2 THz Transmission) of Each Pixel for the Middle Part of A, N and TT corks (continued)

Sample	Mean	Standard Deviation	Skewness	Kurtosis
N11	0.994005	0.075681	1.728375	3.670225
N12	1.022822	0.064676	1.838803	4.353607
N13	1.108755	0.08216	0.954443	0.713991
N14	2.123192	0.319724	0.091455	-1.08993
N15	1.080489	0.070649	1.507151	3.195521
N16	1.132768	0.053247	1.474871	3.607526
N17	1.036393	0.068306	1.642133	4.199732
N18	1.078226	0.056446	1.668111	3.95052
N19	1.009817	0.071726	1.82817	3.9522
N20	0.994516	0.051177	2.031617	5.670375
TT1	2.088504	0.297258	1.005533	1.740495
TT2	1.911499	0.251483	1.650645	4.868913
TT3	1.777123	0.279392	1.725631	3.593975
TT4	1.96459	0.309197	1.718692	4.082192
TT5	1.762139	0.245627	2.019971	6.63276
TT6	2.021429	0.345307	1.936562	5.561361
TT7	1.891509	0.201543	1.028723	2.033007
TT8	1.989813	0.294241	1.706189	4.284267
TT9	1.858657	0.192178	1.209488	2.376984
TT10	1.984773	0.270238	1.358052	2.484526
TT11	2.039557	0.242696	1.095242	1.751517
TT12	1.965654	0.275638	1.500136	3.492129
TT13	1.944857	0.29325	1.681301	4.576682
TT14	2.115065	0.272347	1.023006	1.590804
TT15	2.042747	0.278389	1.084872	1.386062
TT16	1.919743	0.259726	1.592177	3.304025
TT17	1.990033	0.273617	1.617688	4.09234
TT18	1.870823	0.191176	1.166976	2.279531
TT19	1.988129	0.238348	1.213967	2.921542
TT20	1.937613	0.208496	0.651941	0.099741

To eliminate pixels which correspond to the edges scattering the THz beam, only a certain range of pixels are count in the statistics. Ranges are picked depending on the length of the sample and the length of the edges. Also note that only the middle

agglomerated portion of the TT cork samples is compared with the A and N cork results. For the twin top discs, another table is created in Table 3.3.

Table 3.3 Summary Statistics for Absorbance (0.15-0.2 THz Transmission) of Each Pixel for the Twin Top Discs of TT Corks

	Top Disc		Bottom Disc	
Sample	Average	Standard Deviation	Average	Standard Deviation
TT1	1.02142	0.104123	1.753959	0.378566
TT2	1.571084	0.28061	2.111707	0.185954
TT3	1.287729	0.278675	2.658957	0.438144
TT4	1.683175	0.250386	1.636547	0.233023
TT5	1.646268	0.429564	1.772249	0.192688
TT6	1.779501	0.407415	2.741572	0.400399
TT7	1.921219	0.456832	2.569826	0.276024
TT8	1.533774	0.233504	1.542951	0.14471
TT9	1.764365	0.324766	2.874768	0.439183
TT10	1.892815	0.359295	1.947627	0.319688
TT11	1.980321	0.291673	2.094289	0.49765
TT12	1.77885	0.216094	2.790768	0.470727
TT13	1.640657	0.177399	2.017423	0.233915
TT14	1.446095	0.105261	1.832691	0.268997
TT15	1.619979	0.284799	2.513059	0.301522
TT16	1.24199	0.147764	2.26865	0.328072
TT17	1.495322	0.160196	2.11077	0.178526
TT18	1.739943	0.163822	1.96968	0.385338
TT19	1.737913	0.507537	2.661735	0.604703
TT20	1.659723	0.158041	1.869536	0.277202

The mean absorbance and standard deviation data from Table 3.2 are plotted in Figure 3.15. It can be shown that with the exception of the N14 cork sample, all the other N samples exhibit comparable mean absorbance and standard deviations. The values for the A corks are cluster together and distinctly separated from the values for the N corks. This can be explained because their different sizes of granules. As a group, N corks exhibit lower absorbance and a smaller standard deviation. A corks exhibit higher absorbance

(almost a factor of 2) and higher standard deviation (more than a factor of two). TT corks have similar granule size to A corks and exhibit similar absorbance but higher standard deviation. Also note that N14 is clearly an anomaly.

The mean absorbance and standard deviation from Table 3.3 is summarized in Figure 3.16. It can be shown that mean values of the twin top discs of TT corks vary over a wide range. While the mean value may generally characterize the sample, higher mean values may indicate denser cork granules corresponding to smaller cork cells. To understand this feature, one needs to consider possible changes in the cell structure or density that could modify the efficiency of scattering. Typically during the spring, cork trees are growing more rapidly (spring wood), and the cork cells are larger. In comparison, the new cells that are formed during the summer growth are smaller (summer wood) and more densely packed. Moreover, as the tree grows radially and the diameter of the tree expands, the regular pattern of cell cannot be maintained. Consequently, a disruption in the regularity of the cell structure occurs leading to a change in grain structure.[6] Either an increase in cell size or disruption in the grain structure could lead to increased THz scattering and high absorbance. [14]

Figure 3.16 is a chart of mean absorbance value and standard deviation for the twin top discs on TT corks. One can notice that discs with higher mean absorbance value tends to have higher standard deviation. The standard deviation reflects the uniformity of the cork sample. Higher standard deviation means more dispersion from the mean. In other words, the sample is less uniform. It is interesting to note that the ‘top’ disks seem to exhibit a lower absorbance than the ‘bottom’ disks. This variation is unexpected since the

'top' and 'bottom' of the cork, which is defined relative to the hand-written label on each cork sample, should be randomly defined.

Skewness measures the asymmetry of the data. From the table, it can be noticed that the skewness value for all the samples are positive, which means that a pixel's absorbance value is less than the overall average for most of the pixels. This is caused by the fact that there is a minority of pixels which exhibit large absorbance values relative to the mean. Most of the pixels exhibit absorbance values below the mean.

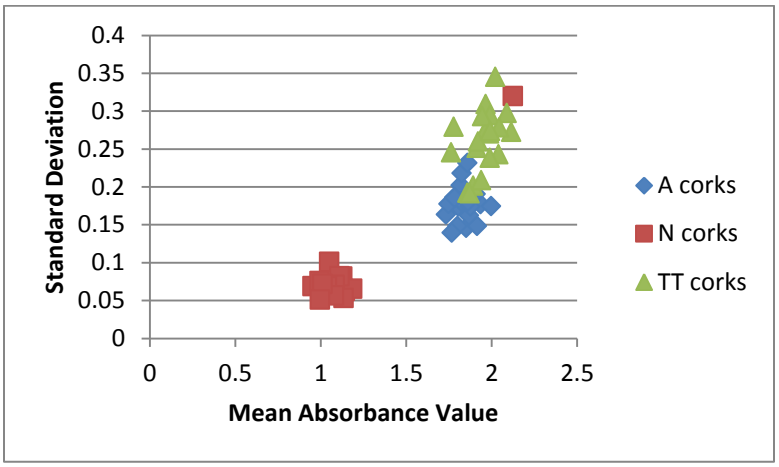

Figure 3.15 Mean absorbance value and standard deviation for all samples

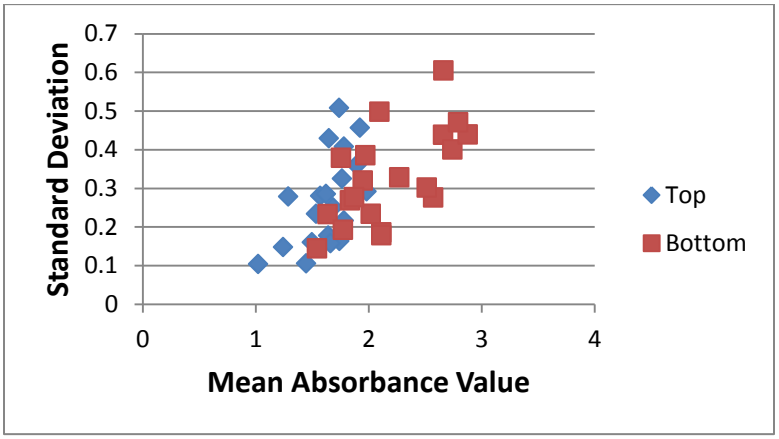

Figure 3.16 Mean absorbance value and standard deviation for the twin top discs

Kurtosis measures the peak of the distribution. It is also an indicator of normality. Positive kurtosis indicates too few cases in the tails or a tall distribution, while negative kurtosis indicates too many pixels in the tails or a flat distribution. [16] It can be shown that most of the samples have a kurtosis of positive value, meaning that they have a tall distribution, in another words, the absorbances of most pixels are concentrated in a narrow range.The same method is applied to the time delay data. Results are listed in Table 3.4. For the twin top discs, results are listed in Table 3.5.

Table 3.4 Summary Statistics for Time delay (ps) of Each Pixel for the Middle Part of A, N and TT corks .

	Average	Standard Deviation	Skew	Kurtosis
A1	14.67162	0.332473	0.006403	0.289951
A2	15.27301	0.333636	0.118505	0.1575
A3	15.2957	0.319923	0.561799	0.24056
A4	14.93593	0.289072	0.215587	-0.085
A5	15.36101	0.341792	0.137865	0.184122
A6	15.5012	0.298395	-0.03127	0.08688
A7	15.30432	0.339588	0.153244	-0.06269
A8	15.1892	0.327154	0.053251	-0.2619
A9	14.80172	0.33032	0.143219	-0.04668
A10	14.80733	0.280102	0.061319	0.007627
A11	15.49094	0.377986	0.14742	-0.04728
A12	15.17927	0.342754	-0.68529	0.580377
A13	15.09761	0.306362	0.051029	-0.16106
A14	14.63916	0.294597	0.070302	-0.09907
A15	14.92404	0.259373	0.017573	-0.18124
A16	15.32437	0.3113	-0.01958	-0.06564
A17	14.63031	0.295121	-0.32571	0.294469
A18	15.50133	0.324568	0.054709	0.114293
A19	15.24995	0.356654	3.429977	92.4607
A20	15.08523	0.362504	0.617313	0.215799
N1	13.83031	0.20793	0.239192	-0.13168
N2	13.80365	0.614119	0.894755	-0.4555
N3	13.724	0.184565	0.160848	-0.17365
N4	13.14514	0.216647	0.491244	-0.28084

Table 3.4 Summary Statistics for Time delay (ps) of Each Pixel for the Middle Part of A, N and TT corks (Continued)

	Average	Standard Deviation	Skew	Kurtosis
N5	13.05437	0.268557	-0.07124	-0.56195
N6	13.7881	0.559802	1.34	0.963493
N7	13.42749	0.173874	0.216444	0.053999
N8	13.46492	0.202039	0.558429	0.945373
N9	13.23365	0.230734	0.603567	0.018492
N10	15.14382	0.346951	0.287705	-0.69081
N11	12.92399	0.213373	0.344914	-0.07158
N12	13.12913	0.191489	0.479911	-0.01477
N13	14.28256	0.452165	0.782231	-0.38322
N14	14.78559	0.917969	0.586271	-1.00282
N15	15.05377	0.349073	1.196444	0.848511
N16	13.69606	0.183587	0.270163	-0.2307
N17	13.44139	0.238159	0.408177	-0.00583
N18	13.37016	0.243082	0.238842	-0.57485
N19	13.16655	0.166092	0.516823	0.252417
N20	13.09946	0.238699	0.663697	0.090104
TT1	15.2948	0.809062	-6.50131	64.83982
TT2	15.2797	0.537141	4.171214	110.7074
TT3	14.78851	0.328184	0.172165	-0.00495
TT4	15.97792	1.027139	1.806106	61.55063
TT5	15.28383	0.541595	-0.07742	-0.31621
TT6	16.6902	1.488459	6.227193	40.86119
TT7	15.2339	0.572439	8.364834	157.6679
TT8	16.20549	0.455232	-3.82224	73.55113
TT9	15.0167	0.419075	0.247538	-0.26839
TT10	16.15373	0.482058	-0.17076	-0.01445
TT11	16.36429	0.527937	1.970898	31.56911
TT12	15.75953	0.386259	0.324101	0.192297
TT13	15.94818	0.429178	-0.23015	0.076193
TT14	16.67768	0.456705	-0.23695	0.221013
TT15	15.35372	0.542473	-0.11945	-0.16499
TT16	15.04495	0.4349	-2.2201	39.70308
TT17	15.84304	0.54856	-0.64589	0.718539
TT18	16.27262	0.434346	-0.86079	1.752447
TT19	15.49059	0.494847	0.269059	-0.20708
TT20	16.56209	0.416182	-0.06474	0.399132

Table 3.5 Summary Statistics for Time Delay (ps) of Each Pixel for the Twin Top Discs of TT Corks

	Top Discs		Bottom Discs	
Sample	Average	Standard deviation	Average	Standard deviation
TT1	7.198099	0.195439	8.045179	0.35587
TT2	9.523714	0.465343	9.409708	1.127103
TT3	6.586963	0.260664	10.49758	1.558428
TT4	8.672235	0.669869	8.442202	2.283142
TT5	8.672466	2.645298	8.5968	0.466159
TT6	12.71806	4.87405	14.31702	3.519189
TT7	13.42365	2.581183	13.83979	1.167914
TT8	8.427294	1.898947	8.395253	0.689382
TT9	10.70791	1.73752	13.98543	2.685584
TT10	11.42288	4.349649	8.980142	2.6286
TT11	9.634015	2.431152	8.755543	5.88069
TT12	9.318985	3.497875	14.25631	2.879334
TT13	9.634015	2.431152	9.34162	5.246862
TT14	8.327799	0.762948	6.862189	0.372402
TT15	8.895872	2.549474	11.05256	5.274552
TT16	7.289422	0.231231	10.36025	0.498921
TT17	10.11842	0.313073	8.909517	0.412046
TT18	10.97045	3.679144	11.78468	7.543126
TT19	7.796838	4.574074	15.99475	14.27861
TT20	8.778087	1.560585	8.442815	1.684841

Figure 3.17 is a chart of mean time delay and standard deviation for all samples. As a group, N corks exhibit lower time delay. A corks exhibit higher time delay. TT corks are similar to A corks, but exhibit higher mean time delay and standard deviation. Unlike the absorbance, no relation between mean value and standard deviation seems to exist for the time delay data. The high standard deviation which TT4 and TT6 corks exhibit may indicate their non-uniformity.

Also note that N2, N6, N10, N13, N14 and N15 samples are distinguished from the rest of the N corks. It will be interesting to see if the differentiation of the N2, N6, N10,

N13, N14 and N15 corks is correlated with the measured oxygen transfer rates. Experimentally measured rates for the agglomerated corks should be available in May 2012.

Figure 3.18 is a chart of mean time delay and standard deviation for the twin top discs. No strong relation between mean time-delay value and standard deviation seems to exist. The bottom disc of TT19 cork exhibits both high time delay value and standard deviation.

Figure 3.19 is a chart of mean absorbance value and mean time delay value for all samples. For A and TT corks, samples are cluster together while for N corks, most of the samples are cluster together with lower absorbance and time delay than A and TT corks except for N10, N14 and N15.

In conclusion, the statistics for absorbance and time-delay can be used to broadly classify the A, N, and TT corks. In the future, the statistical analysis of the THz absorbance and time delay will be correlated with the samples' oxygen transfer rate. The oxygen transfer data will be measured in the Spring of 2012.

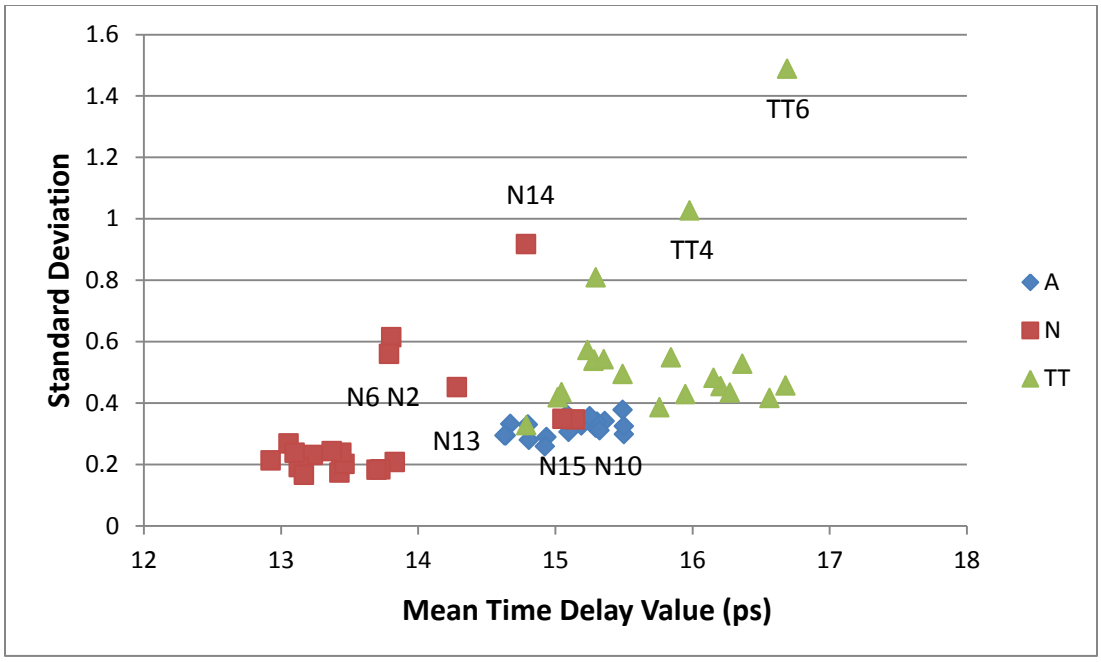

Figure 3.17 Mean time delay value and standard deviation for all samples

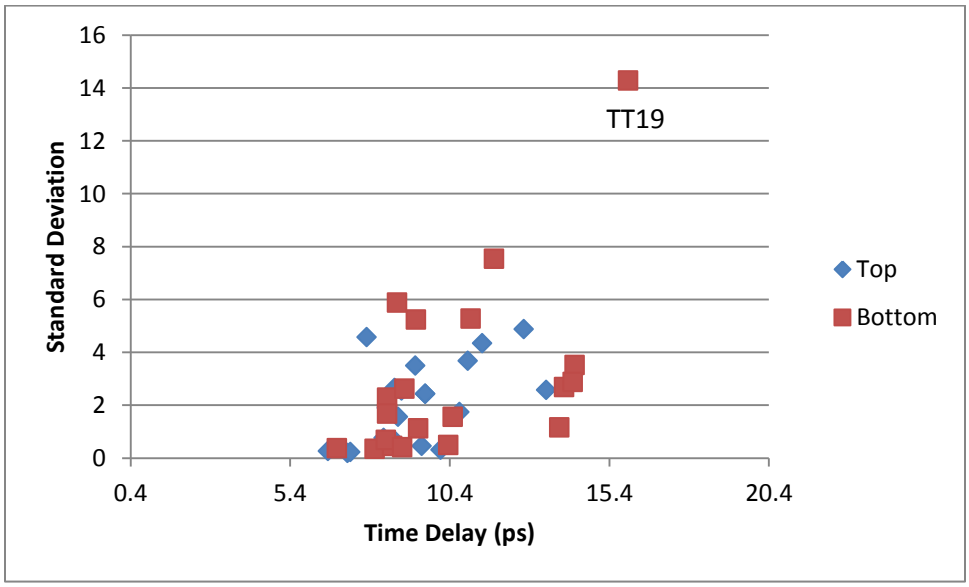

Figure 3.18 Mean time delay value and standard deviation for the twin top discs

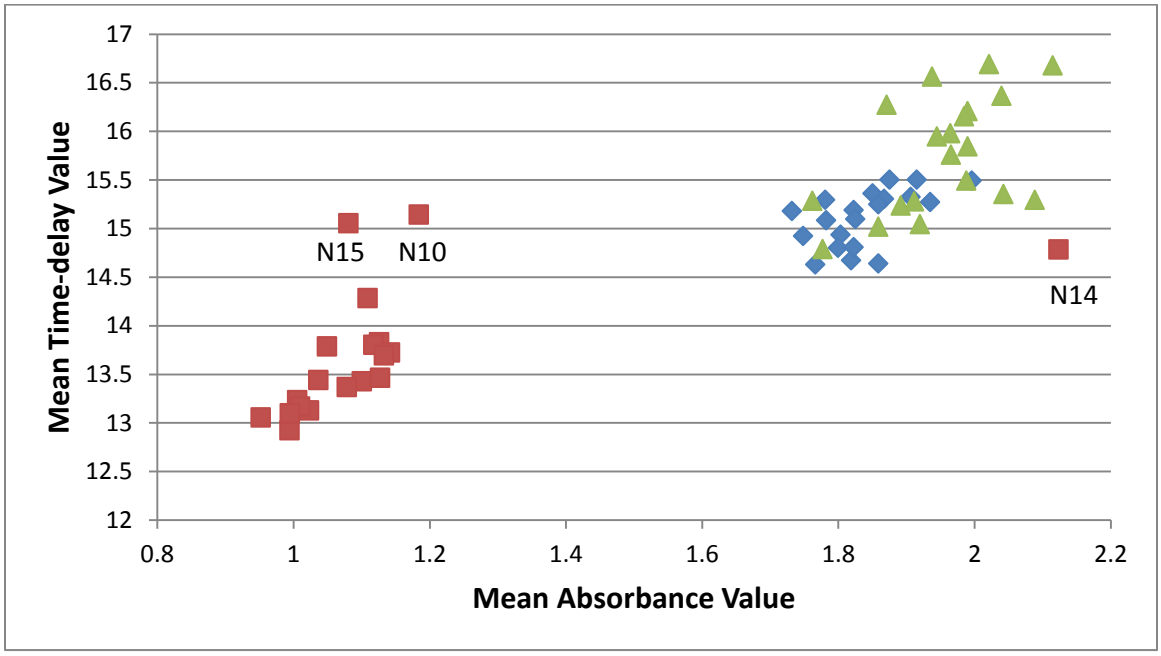

Figure 3.19 Mean absorbance value and mean time delay value for all samples

3.3.3 Polynomial Regression Classification

The first step in this analysis is to calculate the average frequency dependent absorbance between 0.05 to 0.3 THz for all valid pixels on one sample. Then the polynomial regression of Eq. 3.3 is applied and the extracted parameters are analyzed. Parameters are listed in Table 3.6. Some typical polynomial regressions are plotted in Figure 3.19.

From Figure 3.20 it can be shown that for sample TT17, whose B parameter is negative, the absorbance spectra exhibit peaks at around 0.25 THz. Such feature may be caused by the typical type of cork granules or the glues.

Table 3.6 Parameters Extracted from the Polynomial Regression

Sample	B	C	D
A1	21.42808	5.268656	0.051955
A2	0.513916	10.87788	-0.22129
A3	24.10199	4.562631	0.070583
A4	20.38779	6.051741	-0.04866
A5	4.629942	9.930197	-0.19522
A6	23.88313	5.114853	0.085565
A7	18.35607	6.166687	0.01183
A8	24.64472	4.066443	0.136683
A9	10.93397	7.504121	-0.06736
A10	22.99627	4.521663	0.049246
A11	7.827741	9.206026	-0.11316
A12	18.67086	5.480696	-0.00295
A13	11.55129	7.358741	-0.04991
A14	18.11633	6.18055	-0.00113
A15	11.13758	7.320608	-0.072
A16	6.505936	8.95487	-0.10694
A17	10.95423	7.207877	-0.05493
A18	19.80955	5.875163	0.035014
A19	2.004511	10.24978	-0.20174
A20	19.20544	5.881845	-0.03095
N1	7.864172	3.936952	0.145531
N2	11.61302	3.001282	0.179676
N3	11.51828	3.469554	0.129671
N4	10.36173	2.827884	0.143917
N5	7.090905	3.833737	0.028632
N6	12.70539	2.338727	0.196846
N7	10.61115	3.048495	0.179556
N8	8.185006	3.939904	0.135865
N9	10.77105	2.940489	0.123075
N10	16.20811	2.011127	0.25437
N11	6.244535	4.421528	-0.00855
N12	8.815261	3.218997	0.140759
N13	14.31629	2.635346	0.153085
N14	25.93251	-2.52954	0.659331
N15	14.55775	2.324031	0.173394
N16	9.935718	3.588861	0.149857
N17	10.58996	3.05747	0.135341
N18	9.520609	3.389484	0.145393

Table 3.6 Parameters Extracted from the Polynomial Regression (Continued)

Sample	B	C	D
N19	11.63237	2.329404	0.195147
N20	7.754524	3.526378	0.099089
TT1	13.84539	7.120277	0.008397
TT2	-12.4436	12.20175	-0.24411
TT3	10.37249	6.67075	-0.03107
TT4	-12.8244	12.63421	-0.25341
TT5	7.304497	6.94835	-0.01987
TT6	-9.10899	12.43284	-0.26655
TT7	-7.70593	11.39372	-0.24329
TT8	16.19821	6.134782	0.030048
TT9	0.834676	9.404967	-0.16981
TT10	19.65292	4.780075	0.155744
TT11	16.181	6.058539	0.097719
TT12	10.12215	7.792153	-0.04959
TT13	9.780729	7.737079	-0.06487
TT14	-9.91721	12.67223	-0.20311
TT15	-16.1317	14.13197	-0.34181
TT16	14.70765	6.144464	0.030475
TT17	-24.0419	15.68133	-0.41072
TT18	-2.67896	9.80754	-0.10773
TT19	-2.8528	10.96146	-0.21702
TT20	19.52098	4.629443	0.161545

The frequency dependent absorbance can be modeled with Mie scattering theory.[16,17] In the usual case, absorbance can be well described by a second order polynomial (as shown in Figure 3.20 left) with the second order coefficient positive. Parameter B of Eq. 3.3 determines the curvature. Parameters B and C together decide the absorbance growth rate. While it is not certain that the classification of the B and C parameters of the polynomial fit to the average spectral data will be correlated to the oxygen transfer rates, one can use these parameters to differentiate among the various cork samples. For example, the following corks share similar parameters: A1, A3, A4, A6, A7, A8, A10, A12, A14, A18 and A20.

Figure 3.21 is a chart of parameters B and C. As shown in the figure, there exists a linear relationship between parameter B and C for most of the cork samples. A and TT corks share the similar linear function. N corks have a similar slope but lower y-intercept. The N14 sample exhibits a negative C coefficient indicating a negative curvature to the spectral absorbance.

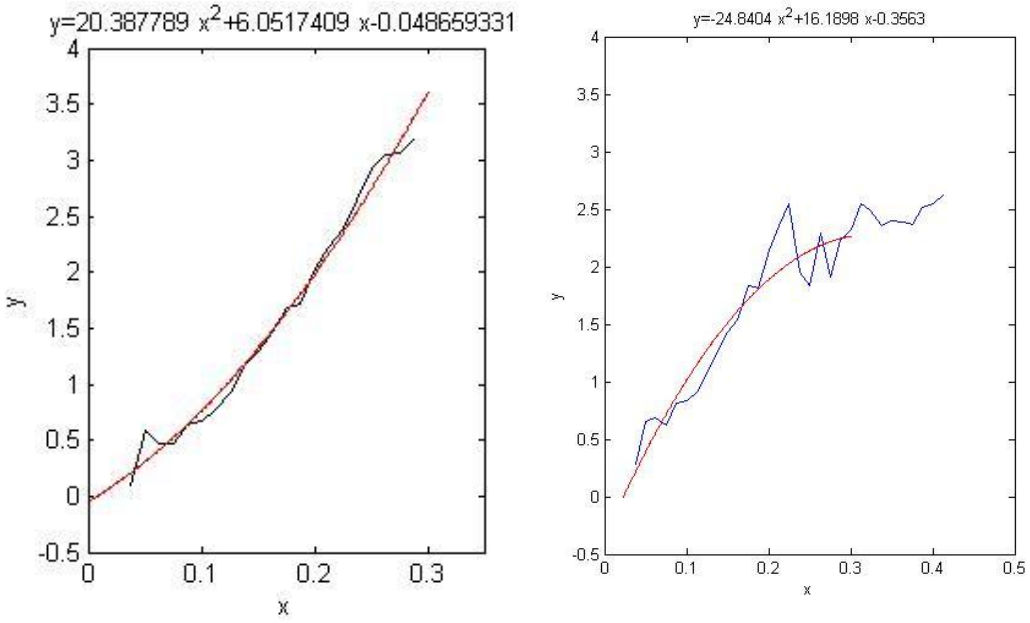

Figure 3.20 Average absorbance (black) and its second order polynomial regression (red) for sample A4 (left) and TT17 (right). X is frequency (THz) and y is Absorbance.

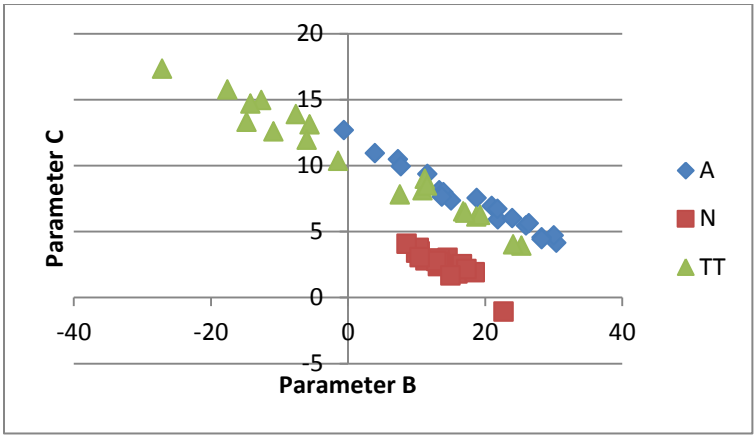

Figure 3.21 Parameters B and C for all samples

CHAPTER 4

CONCLUSIONS AND FUTURE OUTLOOK

After about 30 decades of development, THz science and technology is becoming more refined and practical. Both THz spectroscopy and THz imaging techniques have evolved into versatile tools for the fundamental study of materials and for the realization of a myriad of applications. In this thesis, these techniques were applied to the quality assessment field. Taking advantage of its unique feature of non-destructive, penetrating radiation as well as its strong high interaction with the cork's internal structure, THz spectroscopy and imaging techniques are applied to non-destructive evaluation of agglomerated wine corks.

In this thesis, THz spectroscopy and THz imaging techniques were used to measure 60 agglomerated cork product samples, and demonstrate the feasibility of classifying the corks using THz spectroscopy and imaging. The THz data are analyzed in three ways. Using a time-domain THz spectroscopy and imaging system, THz transmission in the 0.15-0.2 THz range is used to generate images based on either absorbance of the THz radiation or time-delay of the THz pulses. The contrast of the THz image shows the presence of internal structure in the corks. In this specific frequency band, the statistical variations of pixels in the image are calculated to help classify the different corks. By this method, N corks show a relatively low absorbance compared to A or TT corks. The absorbance values for A and TT corks are comparable. This can be understood by the fact

that the N corks have smaller cork granule sizes compared to the A and TT corks. The smaller cork granules lead to more uniform structural properties and less scattering.

A third method of classification uses the average spectral shape of the THz absorbance to calculate the curvature of the absorbance as a function of frequency. A second order polynomial regression is applied and the fit parameters are extracted and analyzed. For A and TT corks, linear and quadratic fit parameters generally obey the same linear relationship while for N corks, parameter B and C obey a linear relationship with similar slope but lower y-intercept.

Based on the analysis of the THz data thus far, there appears to be several parameters which can be used to classify the corks. However, the work and analysis in this thesis does not complete the task of classification. The next step of this work should be to correlate the THz results with experimentally measured oxygen transfer rates for each cork. The oxygen data will take approximately 6 months to complete. After measuring the oxygen transfer rate of each sample, one can explore the relationship between the THz classification and the measured oxygen transfer rates for the different cork groups.

The ultimate goal for the quality assessment of agglomerated cork products is to infer the oxygen transfer rate of the sample based on the THz absorbance and time-delay images. If one were able to correlate the cork's THz images to oxygen transfer rates, then THz imaging could be used as a fast, non-invasive, non-destructive evaluation alternative for agglomerated cork products. In the longer term, the non-destructive evaluation method could potentially be adapted to the cork manufacturing process enabling non-destructive, automatic quality assessment of agglomerated cork products in the factory.

REFERENCES

1. Jansen, C., et al., *Terahertz imaging: applications and perspectives.* Appl. Opt., 2010. **49**(19): p. E48-E57.

2. Mittleman, D., *Sensing with terahertz radiation*. Springer (Berlin, Germany) 2003.

3. Nagatsuma, T., *Terahertz technologies: Present and future.* IEICE Electronics Express, 2011. **8**(14): p. 1127-1142.

4. Siegel, P.H., *Terahertz technology in biology and medicine.* IEEE Transactions on Microwave Theory and Techniques, 2004. **52**(10): p. 2438-2447.

5. M.J. Fitch and R. Osiander, Johns Hopkins *APL Technical Digest*, **25**, 348 (2004)

6. Pereira, H., *Cork: Biology, Production and Uses*, Elsevier (New York) 2007.

7. Agglomerated Cork Stoppers, Cork in Portugal, Retrieved November 16, 2011 from the World Wide Web: http://www.cork.pt/agglomerated-cork-stoppers.html

8. Wine Guide: Tasting Wine, My Wines Direct, Inc., Retrieved November 16, 2011 from http://www.mywinesdirect.com/my-wine-guide/wine-tasting

9. J. Chang, G. Han, J. M. Valverde, N. C. Griswold, J. F. Duque Carrillo, and E. Sanchez-Sinencio, "Cork quality classification system using a unified image processing and fuzzy-neural network methodology," *IEEE Trans. Neural Netw.* **8**, 964-974 (1997).

10. R. Juanola, D. Subira, V. Salvado, J. A. Garcia Regueiro, and E. Antico, "Evaluation of an extraction method in the determination of the 2,4,6-trichloroanisole content of tainted cork," *J. Chromatogr. A* **953**, 207-214 (2002).

11. E. Lizarraga, A. Irigoyen, V. Belsue, and E. Gonzalez-Penas, "Determination of chloroanisole compounds in red wine by headspace solid-phase microextraction and gas chromatography-mass spectrometry," *J. Chromatogr. A* **1052**, 145-149 (2004).

12. E. Herve, S. Price, G. Burns, and P. Weber, presented at the ASEV Annual Meeting, Reno, Nevada, 2 July 1999. http://www. Corkqc.com/asev/asev2-2.htm.

13. A. Brunetti, R. Cesareo, B. Golosio, P. Luciano, and A. Ruggero, "Cork quality estimation by using Compton tomography," *Nucl. Instrum. Methods Phys. Res. B* **196**, 161-168 (2002).

14. Y. L. Hor, J. F. Federici, and R. L. Wample, 'Non-destructive evaluation of cork enclosures using terahertz/ millimeter wave spectroscopy and imaging', *Appl. Optics* **47**, 72-78 (2008)

15. Anthony J. Teti & David E. Rodriguez & John F. Federici & Caroline Brisson 'Non-Destructive Measurement of Water Diffusion in Natural Cork Enclosures Using Terahertz Spectroscopy and Imaging', J Infrared Millimeter and Terahertz Waves (2011) **32**, 513–527

16. Oscar Torres, Descriptive Statistics Using Excel and Stata, Retrieved November 16, 2011 from http://www.princeton.edu/~otoorres/Excel/excelstata.htm

17. Hor, Y.L., J.F. Federici, and R.L. Wample, *Nondestructive evaluation of cork enclosures using terahertz/millimeter wave spectroscopy and imaging.* Applied Optics, 2008. **47**(1):p. 72-78.

18. Bandyopadhyay, A., et al., *Effects of scattering on THz spectra of granular solids.* International Journal of Infrared and Millimeter Waves, 2007. **28**(11):p. 969-978